Available online at www.sciencedirect.com
SCIENCE DIRECT
Precambrian Research 146 (2006) 179–212
Precambrian Research
www.elsevier.com/locate/precamres

Reworking of juvenile crust: Element and isotope evidence from Neoproterozoic granodiorite in South China

Rong-Xin Wu [a,b], Yong-Fei Zheng [a,c,*], Yuan-Bao Wu [a], Zi-Fu Zhao [a], Shao-Bing Zhang [a], Xiaoming Liu [b], Fu-Yuan Wu [c]

[a] CAS Key Laboratory of Crust-Mantle Materials and Environments, School of Earth and Space Sciences, University of Science and Technology of China, Hefei 230026, China
[b] MOE Key Laboratory of Continental Dynamics, Department of Geology, Northwest University, Xi'an 710069, China
[c] State Key Laboratory of Lithosphere Evolution, Institute of Geology and Geophysics, Chinese Academy of Sciences, Beijing 100029, China

Received 23 June 2005; received in revised form 26 January 2006; accepted 27 January 2006

Abstract

A combined study of geochronology and geochemistry was carried out for Neoproterozoic granodiorites at the southeastern margin of the Yangtze Block in South China. The results demonstrate that sedimentary rocks derived from juvenile crust were melted to form strongly peraluminous granite in an arc-continent collision zone, resulting in continental growth. LA-ICPMS zircon U-Pb dating yields two groups of age at 824 ± 6 and 882 ± 16 Ma, respectively. From CL images, the young zircons are new grains or rims of homogeneous structure with magmatic zoning, whereas most of the old ages occur in cores or as single xenocrysts. The granodiorites show high A/CNK ratios of 1.38–1.89 and strong negative Nb and Ta anomalies as well as high $\delta^{18}O$ values of 11.9–14.0‰ for quartz and 8.1–10.2‰ for zircon, pointing to a supracrustal origin characteristic of S-type granites. On the other hand, they have positive $\varepsilon_{Hf}(t)$ values of 3.4 ± 1.6 to 5.4 ± 2.6 for zircon, neutral $\varepsilon_{Nd}(t)$ values of -2.06 to 0.02 and low to medium initial $^{87}Sr/^{86}Sr$ ratios of 0.7033–0.7087 for whole-rock, indicating a magmatic source with significant components of juvenile crust similar to I-type granites. Relatively refractory minerals like zircon, garnet and quartz retain their magmatic O isotope ratios, whereas the other minerals, such as K-feldspar, plagioclase and biotite that show O isotopic disequilibria when paired with quartz, suffered different degrees of post-magmatic alteration at subsolidus temperatures. On the basis of element and isotope geochemistry, we interpret the 882 ± 16 Ma zircons as being inherited from arc-derived igneous rocks, and the 824 ± 6 Ma zircons as having crystallized from an anatectic crustally-derived magma. Arc-continent collision is inferred to have taken place at ca. 900 ± 20 Ma during assembly of the supercontinent Rodinia. Subsequent to weathering of juvenile crust in the back-arc basin, low-maturity sedimentary rocks were deposited from about 880 to 830 Ma between the Yangtze and Cathaysia Blocks. Extensional collapse of the collisional orogen at about 830–820 Ma is suggested as a geodynamic mechanism for burial and melting of the sediments of juvenile crust to produce the S-type granodiorites. As a result, the granodiorites are characterized by the features of both S- and I-type granites, and thus testify to the short-term recycling of juvenile crust with significant contributions to continental growth. The syn- and post-collisional magmatism may be a basic mechanism to result in compositional evolution from arc crust to continental crust.

Keywords: Peraluminous granite; Geochronology; Geochemistry; Petrogenesis; Arc-continent collision; Continental growth; Extensional collapse

1. Introduction

Granite is the most important component of continental crust, recording information about its formation

* Corresponding author. Tel.: +86 5513603554; fax: +86 5513603554.
E-mail address: yfzheng@ustc.edu.cn (Y.-F. Zheng).

0301-9268/$ – see front matter © 2006 Elsevier B.V. All rights reserved.
doi:10.1016/j.precamres.2006.01.012

and evolution in the processes of plate convergence and mantle upwelling. This issue has become particularly pertinent for Neoproterozoic igneous rocks in South China because their origin is closely associated with assembly and breakup of the supercontinent Rodinia. Recent studies of geochronology and geochemistry on these rocks hypothesize that granitoid rocks crystallized at ca. 830–740 Ma in the periphery of the Yangtze Block may petrogenetically be related to the Rodinia breakup that could be triggered by a mantle superplume event (Li et al., 1999, 2003a, 2003b). In view of trace element compositions, however, this genetic hypothesis has been challenged and an alternative scenario of island-arc origin has been proposed for some of Neoproterozoic igneous rocks (Zhou et al., 2002a, 2002b, 2004; Wang et al., 2004a, 2004b). Basic questions remain as to how to identify the contribution of energy and material from a mantle plume (or superplume) in granite petrogenesis and how to distinguish igneous rocks of island-arc origin from those derived from crustal melting in collision orogens. If no coeval mantle-derived material was added to granitoid magmas, extensional collapse of orogens may be a viable mechanism for generation of post-collisional granitoids (Dewey, 1988).

Neoproterozoic granodiorites at the southeastern margin of the Yangtze Block, particularly those geographically located in the southern part of Anhui province (South Anhui hereafter), have been one of the important targets for this controversy. Previous petrological and geochemical investigations show that they have high ratios of molecular $Al_2O_3/(CaO + Na_2O + K_2O)$, or A/CNK ratios, of 1.1–1.5 with the occurrence of cordierite (Li et al., 2003a), pointing to a sedimentary source that experienced chemical weathering. On the other hand, neutral $\varepsilon_{Nd}(t)$ values of −1.7 to −0.2 and low initial $^{87}Sr/^{86}Sr$ ratios of 0.70392 ± 0.00033 were obtained (Zhou and Wang, 1988; Li et al., 2003a), indicating a magmatic source with significant components of juvenile crust. These contrasting features provide us with a good opportunity to study the recycling of juvenile crust and its contribution to continental growth, with a potential resolution to the genetic controversy concerning the Neoproterozoic granitoids in South China. This paper presents a combined study of zircon U–Pb dating and Lu–Hf isotopes, whole-rock elements and Sr–Nd isotopes, and mineral O isotopes for the Neoproterozoic granodiorites in South Anhui.

Zircon is a refractory mineral that forms a highly robust phase in many geological environments and thus is readily amenable to methods of radiometric dating and geochemical tracing (Hanchar and Hoskin, 2003). Igneous zircons commonly have complex internal structures and may record the multistage evolution of their host rocks. Thus a combined study of in situ U–Pb dating and cathodoluminescence (CL) imaging can be used to decipher their protolith age and history. Furthermore, application of Hf isotopes in zircon has been well developed recently to trace igneous rock origin and the evolution of crust and mantle over time (e.g., Amelin et al., 1999, 2000; Griffin et al., 2000, 2002; Andersen et al., 2002; Samson et al., 2003; Zheng et al., 2006). The Sm–Nd isotope method is also a means of acquiring the average age of crustal residence (e.g., Jacobsen, 1988; DePaolo et al., 1991), and can be used to distinguish between juvenile young and recycled ancient crusts. On the other hand, the O isotope geochemistry of crust-derived magmas can reflect the long term mixing of mantle-derived melts with the crust, with a particular advantage for identification of surface water (Hoefs, 2004). Magmatic zircon has been demonstrated to be capable of preserving its igneous $\delta^{18}O$ value through subsolidus hydrothermal alteration and granulite-facies metamorphism (Valley, 2003; Zheng et al., 2004), so that the zircon O isotope method can be used to trace the geochemical nature of its magmatic source. This study has taken full advantage of these different approaches for the purpose of solving the problems concerning the origin of granites. The results indicate that orogenic belts formed by arc-continent collisions contain invaluable records of the continental growth and evolution.

2. Geological setting and samples

The South China Craton consists of the Yangtze and Cathaysia Blocks lying to the northwest and southeast, respectively, of the Jiangshan-Shaoxing fault that is bounded by the Jiangnan Fold Belt (inset in Fig. 1). Subduction of ocanic crust during the Late Mesoproterozoic to Early Neoproterozoic is commonly assumed for convergence between the two blocks, with arc-continent and/or continent–continent collisions postulated between them (e.g., Charvet et al., 1996; Zhao and Cawood, 1999; Li et al., 2002a; Li and Li, 2003). The Neoproterozoic granodiorites in South Anhui are located in the eastern part of the Jiangnan Fold Belt between the Yangtze and Cathaysia Blocks (Fig. 1). They have a total outcrop area of ca. 200 km^2, and include three intrusives: the Xucun (133 km^2), Xiuning (32 km^2) and Shexian (32 km^2) plutons. They intrude the Shangxi Group, a sequence of low-grade metasediments of late Mesoproterozoic to early Neoproterozoic age, but are unconformably overlain by middle Neoproterozoic sediments of the Xiuning Formation (Wang and Li, 2003). All three plutons consist of biotite-rich, cordierite-bearing gran-

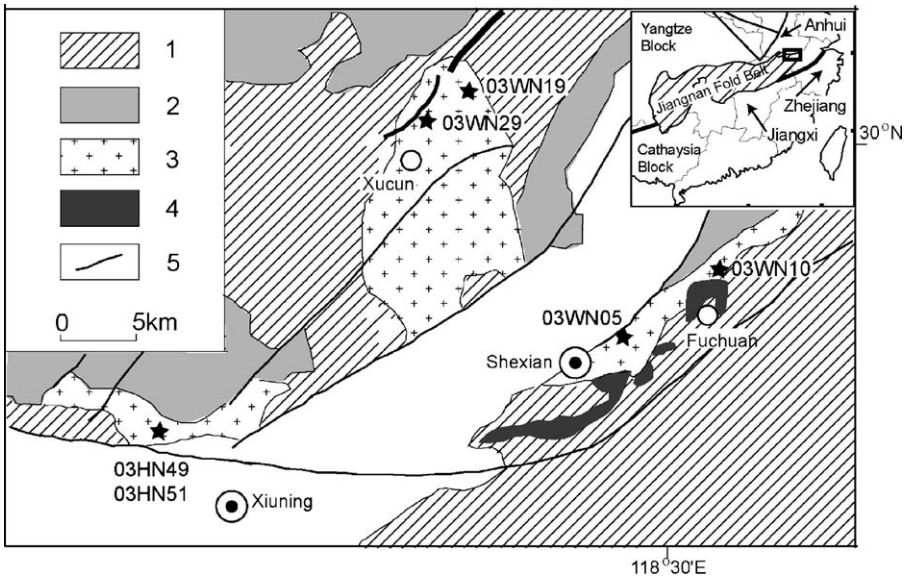

Fig. 1. Simplified geological map showing the distribution of Neoproterozoic granodiorites in South Anhui (inset shows their position between the Yangtze and Cathaysia Blocks in South China). Asterisks close to the sample number denote the locality of samples for zircon U–Pb dating. Number in legend: (1) late Mesoproterozoic to early Neoproterozoic metasediments (the Shangxi Group); (2) middle Neoproterozoic sediments (the Xiuning Formation); (3) Neoproterozoic granodiorite; (4) Neoproterozoic ophiolite; (5) fault. Granite symbols close to the locality name denotes the adjacent pluton, and the unit without ornament represents the Quaternary cover.

odiorites with very similar mineral assemblages (Zhou and Wang, 1988; Xing et al., 1988). The major minerals are quartz, K-feldspar, plagioclase, biotite and cordierite, with minor amounts of secondary muscovite and accessory minerals such as zircon, garnet, apatite, ilmenite and monazite. South of the Shexian pluton (Fig. 1), a Neoproterozoic ophiolite has been identified at Fuchuan which gave Sm-Nd isochron ages of 1024 ± 30 Ma (Zhou et al., 1989) and 935 ± 10 Ma (Chen et al., 1991).

A Rb–Sr isochron age of 964 ± 184 Ma was reported by Zhou and Wang (1988) for the Xiuning pluton. Xing et al. (1988) obtained an averaged $^{207}Pb/^{206}Pb$ age of 928 Ma from two highly discordant U–Pb zircon analyses for the Shexian pluton, and a biotite K–Ar age of 913 Ma for the Xucun pluton. All of these ages were interpreted as being syn-orogenic during the Jinning orogeny in the early Neoproterozoic. However, a SHRIMP zircon U–Pb age of 823 ± 8 Ma has been reported by Li et al. (2003a) for the Xucun pluton, which is interpreted as the time of granodioritic magmatism and thus related to a mantle superplume event during the breakup of the supercontinent Rodinia.

Thirty-three samples were collected from the Xucun, Shexian and Xiuning plutons for analysis of mineral O isotopes, twelve of which were selected for the analyses of whole-rock major and trace elements as well as Sm–Nd and Rb–Sr isotopes, and six of which were further selected for a combined study of zircon U–Pb ages and CL imaging. Of these six samples, two are from the Xucun pluton (03WN19 and 03WN29) in Shangfeng Village (30°00′58″N, 118°20′47″E) and Zhenling Village (30°00′39″N, 118°19′13″E), respectively; two from the Shexian pluton (03WN05 and 03WN10) in Nanyuankou Town (29°52′53″N, 118°28′59″E) and Chencunjiang Town (29°55′31″N, 118°33′19″E), respectively; two are from the Xiuning pluton (03HN49 and 03HN51) near the bridge to the north of Xiuning County (29°50′07″N, 118°09′21″E). Samples from each of the three plutons were selected for zircon Lu–Hf isotope analysis.

3. Analytical methods

All the whole-rock samples of specimen were fresh without visible weathering, but low-T alteration is indicated by chloritisation of biotite and clouding of feldspars. After crushing, the samples were processed by conventional magnetic and density techniques to separate zircons and other minerals. A representative selection of zircons was extracted by hand-picking under a binocular microscope. Zircons were cast in an epoxy mount, which was then polished to section the crystals for analysis. CL images were taken using a JXA-8800R electron microprobe at the Institute of Mineral Resources in the Chinese Academy of Geological Sciences, Beijing.

Zircon U–Pb dating was carried out at the Department of Geology in Northwest University, Xi'an. The GeoLas 200M laser-ablation system equipped with a 193 nm ArF-excimer laser was used in connection with an ELAN6100 DRC ICP-MS. Helium was used as the carrier gas to enhance the transport efficiency of the ablated material. The helium carrier gas inside the ablation cell is mixed with argon as a makeup gas before entering the plasma to maintain stable and optimum excitation conditions. The spot diameter was 30 μm. Each analysis includes a background acquisition interval of approximately 30 s and a signal acquisition of about 80 s. Raw data were processed using the Glitter program to calculate U–Pb ages. All measurements were performed using zircon 91500 as the external standard with a $^{206}Pb/^{238}U$ age of 1065.4 ± 0.6 Ma (Wiedenbeck et al., 1995). The standard silicate glass NIST SRM610 was used to calculate U, Th and Pb concentrations. The detailed analytical method was described by Yuan et al. (2004). The common Pb correction was carried out by using the EXCEL program of ComPbCorr#_151 (Anderson, 2002).

Zircon Hf isotopic analysis was carried out in situ using a Geolas-193 laser-ablation microprobe, attached to a Neptune multi-collector ICP-MS at the Institute of Geology and Geophysics in the Chinese Academy of Sciences, Beijing. Instrumental conditions and data acquisition were as described by Xu et al. (2004). Both He and Ar carrier gases were used to transport the ablated sample from the laser-ablation cell via a mixing chamber to the ICPMS torch. In order to correct the isobaric interferences for ^{176}Lu and ^{176}Yb on ^{176}Hf, the appropriate $^{176}Lu/^{175}Lu$ and $^{176}Yb/^{172}Yb$ ratios were determined, respectively, by successive spiking a solution of JMC 14374 with variable Yb/Hf ratios (Griffin et al., 2000) but with an additional control following the procedures of Iizuka and Hirata (2005) for the Yb–Lu–Hf isotope analyses of five standard zircons (91500, TEMORA, CZ3, CN92-1 and FM0411) that resulted in a reprocessing program for the isobaric interference corrections (Zheng et al., 2006). Zircon 91500 was used as the reference standard, with a recommended $^{176}Hf/^{177}Hf$ ratio of 0.282293 ± 28 (Woodhead et al., 2004). We have adopted a decay constant for ^{176}Lu of 1.865×10^{-11} year^{-1} (Scherer et al., 2001). Initial $^{176}Hf/^{177}Hf$ ratios $\varepsilon_{Hf}(t)$ were calculated with reference to the chondritic reservoir (CHUR) of Blichert-Toft and Albarede (1997) at the time of zircon growth from the magma. Hf model age (T_{DM}) is calculated relative to the depleted mantle with present-day $^{176}Hf/^{177}Hf = 0.28325$ and $^{176}Lu/^{177}Hf = 0.0384$ (Vervoort and Blichert-Toft, 1999).

Major and trace elements, and Sm–Nd and Rb–Sr isotopes were analysed at the Guangzhou Institute of Geochemistry in the Chinese Academy of Sciences, Guangzhou. Major element oxides were determined using a Varian Vista Pro ICP-AES. Trace elements were determined using a Perkin-Elmer Sciex ELAN 6000 ICP-MS. Analyses of USGS rock standards (BCR-2, BHVO-1 and AGV-1) indicate precision and accuracy better than 1% for major elements and 5% for trace elements and REE.

Nd–Sr isotopic compositions were determined using a Micromass IsoProbe multi-collector (MC-ICPMS). The detailed analytical method was described by Li et al. (2002b, 2003a). Measured $^{143}Nd/^{144}Nd$ ratios were normalized to $^{146}Nd/^{144}Nd = 0.7219$, and measured $^{87}Sr/^{86}Sr$ ratios were normalized to $^{86}Sr/^{88}Sr = 0.1194$. Single-stage model ages (T_{DM1}) were calculated relative to the depleted mantle (DePaolo, 1988), and two-stage model ages (T_{DM2}) were calculated relative to the average continental crust with a $^{147}Sm/^{144}Nd$ ratio of 0.118 (Jahn and Condie, 1995).

Oxygen isotope analysis of mineral separates was carried out by the laser fluorination technique using a 25W MIR-10 CO_2 laser at the Laboratory of Chemical Geodynamics in the University of Science and Technology of China, Hefei. O_2 was directly transferred to a Delta+ mass spectrometer for the measurement of O isotope ratios (Zheng et al., 2002). O isotope data are reported as parts per thousand differences (‰) from the reference standard VSMOW in the $\delta^{18}O$ notation. Errors for repeat measurements of each standard on a given day were about ±0.1‰ (1σ) for $\delta^{18}O$. Two reference minerals were used: $\delta^{18}O = 5.8$‰ for garnet UWG-2 (Valley et al., 1995), and $\delta^{18}O = 10.0$‰ for zircon 91500 (Zheng et al., 2004).

4. Results

4.1. Zircon U–Pb ages

Twenty spots were dated for each of the six zircon samples with reference to their CL images. The U–Pb isotope data are listed in Table 1 and some of the CL images are presented in Fig. 2, together with corresponding $^{206}Pb/^{238}U$ ages. For each group of U–Pb isotope data for single samples, a weighted mean of $^{206}Pb/^{238}U$ ages was calculated by means of the ISOPLOT program of Ludwig (2001). The results are presented with 2σ errors in the Wetherill-type concordia diagram (Fig. 3). The scatter in $^{207}Pb/^{235}U$ ratios for each group may be caused by the presence of the variable amounts of the common Pb in a set of cogenetic zircons with differ-

Table 1
LA-ICPMS zircon U–Pb isotope data for Neoproterozoic granodiorites in South Anhui

Sample spot no.	Element (ppm)			Th/U	Isotope ratio						Age (Ma)					
	Th	U	Pb		$^{207}Pb/^{206}Pb$	$\pm1\sigma$	$^{207}Pb/^{235}U$	$\pm1\sigma$	$^{206}Pb/^{238}U$	$\pm1\sigma$	$^{207}Pb/^{206}Pb$	$\pm1\sigma$	$^{207}Pb/^{235}U$	$\pm1\sigma$	$^{206}Pb/^{238}U$	$\pm1\sigma$
03WN19 (Xucun)																
1	56	273	43	0.20	0.06668	0.00119	1.36272	0.02511	0.14827	0.00184	828	19	873	11	891	10
2	91	96	21	0.95	0.07961	0.00234	1.80237	0.05259	0.16420	0.00229	1187	58	1046	18	980	13
3	68	101	17	0.67	0.07000	0.00204	1.31957	0.03819	0.13677	0.00191	928	37	854	17	826	11
4	76	265	40	0.29	0.06845	0.00213	1.29510	0.03671	0.13723	0.00179	882	66	844	16	829	10
5	30	245	73	0.12	0.07072	0.00778	1.39102	0.10117	0.14266	0.00248	949	235	885	46	860	14
6	79	231	42	0.34	0.07150	0.00277	1.39639	0.05076	0.14165	0.00192	972	81	887	22	854	11
7	83	233	39	0.36	0.06969	0.00205	1.39360	0.03684	0.14503	0.00185	919	62	886	16	873	10
8	102	306	51	0.33	0.07288	0.00139	1.46433	0.02858	0.14576	0.00184	1011	20	916	12	877	10
9	57	152	24	0.38	0.07853	0.00183	1.55084	0.03629	0.14326	0.00188	1160	26	951	14	863	11
10	41	215	34	0.19	0.07571	0.00187	1.50942	0.03730	0.14464	0.00193	1087	29	934	15	871	11
11	75	212	34	0.35	0.06802	0.00171	1.35439	0.03419	0.14444	0.00191	869	31	869	15	870	11
12	72	191	32	0.38	0.07054	0.00154	1.41538	0.03137	0.14555	0.00187	944	25	895	13	876	11
13	31	206	30	0.15	0.06707	0.00188	1.26535	0.03155	0.13683	0.00174	840	60	830	14	827	10
14	74	257	40	0.29	0.07069	0.00167	1.34177	0.03187	0.13769	0.00180	948	28	864	14	832	10
15	242	422	70	0.57	0.06948	0.00146	1.32050	0.02822	0.13787	0.00176	913	24	855	12	833	10
16	172	376	57	0.46	0.06734	0.00133	1.25242	0.02485	0.13488	0.00166	848	41	824	11	816	9
17	20	153	25	0.13	0.07399	0.00256	1.47349	0.05052	0.14444	0.00205	1041	70	920	18	870	12
18	75	216	35	0.35	0.06944	0.00211	1.38212	0.03807	0.14435	0.00186	912	64	881	16	869	10
19	111	233	37	0.47	0.06653	0.00134	1.25425	0.02573	0.13677	0.00172	823	23	825	12	826	10
20	216	366	64	0.59	0.06940	0.00137	1.38660	0.02793	0.14493	0.00182	911	22	883	12	872	10
03WN29 (Xuncun)																
1	114	191	35	0.60	0.06694	0.00276	1.30830	0.05105	0.14576	0.00192	778	89	849	22	877	11
2	69	210	33	0.33	0.07095	0.00134	1.33906	0.02582	0.13690	0.00170	956	20	863	11	827	10
3	74	272	42	0.27	0.06603	0.00264	1.20716	0.04531	0.13526	0.00183	766	86	804	21	818	10
4	41	184	27	0.22	0.06507	0.00158	1.21681	0.02962	0.13564	0.00176	777	30	808	14	820	10
5	57	185	32	0.31	0.06652	0.00259	1.32252	0.04767	0.14420	0.00191	823	81	856	21	868	11
6	39	210	44	0.19	0.06545	0.00411	1.29712	0.07740	0.14373	0.00207	789	132	844	34	866	12
7	62	248	40	0.25	0.06674	0.00203	1.31544	0.03630	0.14294	0.00183	830	65	853	16	861	10
8	51	345	65	0.15	0.06707	0.00183	1.40210	0.03967	0.15161	0.00192	840	57	890	12	910	11
9	27	196	33	0.14	0.07995	0.00166	1.34584	0.03443	0.14932	0.00191	786	53	866	13	897	11
10	37	494	78	0.07	0.07788	0.00802	1.45799	0.14536	0.13577	0.00373	1144	205	913	54	821	21
11	51	221	43	0.23	0.07689	0.00241	1.85041	0.05737	0.17456	0.00252	1118	39	1064	20	1037	14
12	226	331	110	0.68	0.09326	0.00123	3.44381	0.04845	0.26784	0.00321	1493	12	1514	11	1530	16
13	209	347	62	0.60	0.07649	0.00147	1.53272	0.03002	0.14534	0.00182	1108	20	944	12	875	10
14	27	205	45	0.13	0.07623	0.00275	1.52736	0.05462	0.14531	0.00196	1101	72	941	15	875	11
15	125	431	116	0.29	0.11183	0.00250	3.40626	0.06336	0.22091	0.00272	1829	41	1506	15	1287	14
16	48	173	29	0.27	0.08270	0.00263	1.56570	0.04896	0.13731	0.00196	1262	62	957	18	829	11
17	60	236	36	0.25	0.07821	0.00166	1.44580	0.03092	0.13409	0.00172	1152	23	908	13	811	10
18	38	188	30	0.20	0.08101	0.00247	1.54058	0.04627	0.13795	0.00199	1222	37	947	18	833	11

Table 1 (*Continued*)

Sample spot no.	Element (ppm)			Th/U	Isotope ratio						Age (Ma)					
	Th	U	Pb		$^{207}Pb/^{206}Pb$	$\pm1\sigma$	$^{207}Pb/^{235}U$	$\pm1\sigma$	$^{206}Pb/^{238}U$	$\pm1\sigma$	$^{207}Pb/^{206}Pb$	$\pm1\sigma$	$^{207}Pb/^{235}U$	$\pm1\sigma$	$^{206}Pb/^{238}U$	$\pm1\sigma$
19	31	214	31	0.15	0.06589	0.00195	1.22902	0.03618	0.13530	0.00186	803	39	814	16	818	11
20	47	167	26	0.28	0.07392	0.00210	1.39548	0.03931	0.13693	0.00190	1039	35	887	17	827	11
03WN05 (Shexian)																
1	68	158	25	0.43	0.06663	0.00183	1.26567	0.03470	0.13777	0.00179	826	57	830	14	832	10
2	127	420	64	0.30	0.06897	0.00184	1.30178	0.03078	0.13688	0.00167	898	56	847	14	827	9
3	29	211	32	0.14	0.06950	0.00198	1.31794	0.03734	0.13753	0.00181	914	59	854	15	831	10
4	155	320	56	0.48	0.06875	0.00238	1.40333	0.04503	0.14804	0.00192	891	73	890	19	890	11
5	123	378	59	0.33	0.06509	0.00126	1.32291	0.02531	0.14741	0.00175	777	21	856	11	886	10
6	98	146	87	0.67	0.15711	0.00222	9.98349	0.14747	0.46092	0.00566	2425	11	2433	14	2444	25
7	42	171	33	0.25	0.07477	0.00201	1.77523	0.04751	0.17221	0.00232	1062	32	1036	17	1024	13
8	124	399	59	0.31	0.06477	0.00219	1.20635	0.03695	0.13508	0.00172	767	71	804	17	817	10
9	70.	353	52	0.20	0.06935	0.00206	1.28110	0.03437	0.13399	0.00170	909	63	837	15	811	10
10	54	271	39	0.20	0.06806	0.00200	1.24126	0.03296	0.13227	0.00167	870	62	819	15	801	9
11	37	157	25	0.24	0.07180	0.00182	1.43815	0.03553	0.14527	0.00185	980	52	905	15	874	10
12	105	122	23	0.86	0.07265	0.00183	1.46955	0.03695	0.14671	0.00192	1004	30	918	15	882	11
13	125	299	52	0.42	0.06809	0.00262	1.30888	0.04733	0.13941	0.00184	871	82	850	21	841	10
14	65	235	35	0.28	0.06829	0.00157	1.29364	0.02977	0.13740	0.00175	877	27	843	13	830	10
15	120	177	31	0.68	0.06823	0.00155	1.38240	0.03149	0.14694	0.00186	876	27	881	13	884	10
16	64	231	35	0.28	0.06746	0.00146	1.28601	0.02803	0.13825	0.00173	852	25	840	12	835	10
17	194	302	51	0.64	0.07310	0.00263	1.38838	0.04649	0.13775	0.00181	1017	75	884	20	832	10
18	108	239	39	0.45	0.06770	0.00328	1.22935	0.05672	0.13170	0.00192	859	103	814	26	798	11
19	233	359	63	0.65	0.06486	0.00128	1.30521	0.02625	0.14594	0.00177	770	23	848	12	878	10
20	99	241	39	0.41	0.06510	0.00246	1.22729	0.04252	0.13673	0.00178	778	64	813	18	826	10
03WN10 (Shexian)																
1	232	549	85	0.42	0.07175	0.00147	1.35408	0.02809	0.13686	0.00171	979	23	869	12	827	10
2	151	479	75	0.32	0.07215	0.00234	1.37267	0.04392	0.13797	0.00198	990	42	877	19	833	11
3	43	260	38	0.17	0.07070	0.00283	1.33923	0.05272	0.13737	0.00214	949	55	863	23	830	12
4	118	395	78	0.30	0.07264	0.00220	1.72953	0.04750	0.17268	0.00221	1004	63	1020	18	1027	12
5	93	289	90	0.32	0.08627	0.00656	2.10953	0.10556	0.17735	0.00301	1344	147	1152	48	1052	16
6	43	276	41	0.15	0.07631	0.00179	1.43934	0.03384	0.13679	0.00177	1103	27	905	14	826	10
7	66	153	25	0.43	0.06753	0.00255	1.27625	0.04494	0.13708	0.00185	854	80	835	20	828	10
8	44	227	33	0.19	0.06622	0.00195	1.22678	0.03253	0.13436	0.00171	813	63	813	15	813	10
9	47	215	34	0.22	0.07187	0.00369	1.32869	0.06503	0.13409	0.00210	982	107	858	28	811	12
10	97	262	44	0.37	0.06887	0.00226	1.37019	0.04119	0.14429	0.00188	895	69	876	18	869	11
11	192	246	48	0.78	0.07856	0.00211	1.64221	0.04671	0.15161	0.00224	1161	53	987	18	910	12
12	61	257	51	0.24	0.06920	0.00611	1.35648	0.11678	0.14616	0.00277	847	188	870	50	879	16
13	151	475	98	0.32	0.07853	0.00282	1.96816	0.06518	0.18176	0.00254	1160	73	1105	22	1077	14
14	99	195	34	0.51	0.07113	0.00186	1.46769	0.03823	0.14965	0.00200	961	32	917	16	899	11
15	45	169	28	0.26	0.07306	0.00180	1.50275	0.03701	0.14919	0.00197	1016	29	932	15	896	11
16	45	206	31	0.22	0.06694	0.00255	1.26103	0.04465	0.13663	0.00191	836	81	828	20	826	11
17	78	308	47	0.25	0.06896	0.00240	1.29857	0.04165	0.13658	0.00185	897	74	845	18	825	10

18	50	209	34	0.24	0.07016	0.00498	1.28236	0.08796	0.13257	0.00245	933	150	838	39	802	14
19	112	335	69	0.33	0.06792	0.00421	1.30233	0.07832	0.13907	0.00209	866	132	847	35	839	12
20	49	222	34	0.22	0.06683	0.00486	1.23268	0.08634	0.13378	0.00258	832	156	816	39	809	15
03HN49 (Xiuning)																
1	26	222	31	0.12	0.06806	0.00217	1.22035	0.03522	0.13005	0.00175	870	68	810	16	788	10
2	85	177	28	0.48	0.06727	0.00154	1.35489	0.03118	0.14624	0.00189	846	27	870	13	880	11
3	26	179	26	0.15	0.06614	0.00178	1.24445	0.03346	0.13662	0.00185	811	34	821	15	826	10
4	39	183	27	0.21	0.06349	0.00151	1.19390	0.02859	0.13654	0.00178	725	29	798	13	825	10
5	31	224	32	0.14	0.06695	0.00143	1.26356	0.02732	0.13703	0.00176	836	25	830	12	828	10
6	130	222	36	0.58	0.06842	0.00137	1.28916	0.02615	0.13680	0.00173	881	22	841	12	827	10
7	42	199	32	0.21	0.06577	0.00166	1.34582	0.03397	0.14857	0.00198	799	31	866	15	893	11
8	68	245	45	0.28	0.06829	0.00283	1.37480	0.05272	0.14601	0.00198	877	86	878	21	879	11
9	39	243	38	0.16	0.06866	0.00124	1.39686	0.02588	0.14771	0.00185	889	19	888	11	888	10
10	58	195	29	0.30	0.06161	0.00145	1.15879	0.02742	0.13658	0.00177	661	29	781	13	825	10
11	25	314	44	0.08	0.06515	0.00165	1.20436	0.02642	0.13408	0.00168	779	54	803	12	811	10
12	78	254	44	0.31	0.06936	0.00264	1.42861	0.04969	0.14939	0.00204	909	78	901	19	898	11
13	65	249	37	0.26	0.06295	0.00149	1.19297	0.02834	0.13761	0.00180	707	29	797	13	831	10
14	34	183	26	0.18	0.06302	0.00165	1.17582	0.03080	0.13548	0.00182	709	33	789	14	819	10
15	54	237	34	0.23	0.06353	0.00186	1.20110	0.03502	0.13730	0.00189	726	39	801	16	829	11
16	64	279	45	0.23	0.06992	0.00137	1.46890	0.02937	0.15258	0.00194	926	21	918	12	915	11
17	32	196	28	0.16	0.06379	0.00142	1.20533	0.02714	0.13724	0.00178	735	26	803	12	829	10
18	69	187	29	0.37	0.06399	0.00148	1.21196	0.02828	0.13755	0.00180	741	28	806	13	831	10
19	38	195	28	0.19	0.06286	0.00144	1.19459	0.02766	0.13803	0.00181	703	28	798	13	834	10
20	34	225	32	0.15	0.06286	0.00157	1.18404	0.02960	0.13681	0.00182	703	31	793	14	827	10
03HN51 (Xiuning)																
1	48	198	31	0.24	0.06619	0.00176	1.26440	0.03348	0.13849	0.00184	812	33	830	15	836	10
2	39	237	35	0.17	0.06688	0.00226	1.25847	0.03905	0.13648	0.00184	834	72	827	18	825	10
3	58	209	31	0.28	0.06512	0.00236	1.23993	0.04432	0.13804	0.00201	778	51	819	20	834	11
4	67	175	45	0.38	0.08598	0.00176	2.64119	0.05471	0.22271	0.00285	1338	21	1312	15	1296	15
5	38	170	25	0.23	0.06576	0.00177	1.24593	0.03337	0.13737	0.00181	799	34	822	15	830	10
6	58	203	32	0.28	0.06706	0.00331	1.28153	0.06196	0.13855	0.00234	840	72	838	28	836	13
7	43	158	24	0.27	0.06773	0.00244	1.27760	0.04267	0.13681	0.00185	860	77	836	19	827	10
8	32	149	22	0.21	0.06921	0.00224	1.31895	0.04205	0.13817	0.00198	905	42	854	18	834	11
9	86	205	33	0.42	0.06652	0.00173	1.26731	0.03297	0.13815	0.00183	823	33	831	15	834	10
10	19	124	18	0.15	0.06655	0.00209	1.26240	0.03923	0.13754	0.00191	824	42	829	18	831	11
11	49	263	37	0.19	0.06513	0.00140	1.18374	0.02568	0.13180	0.00166	779	25	793	12	798	9
12	90	319	53	0.28	0.07229	0.00311	1.30054	0.05207	0.13048	0.00178	994	87	846	21	791	10
13	35	329	47	0.11	0.06508	0.00118	1.22795	0.02284	0.13683	0.00168	777	20	813	10	827	10
14	68	178	31	0.38	0.06544	0.00158	1.37295	0.03319	0.15215	0.00197	789	29	877	14	913	11
15	39	147	23	0.27	0.06775	0.00172	1.28257	0.03263	0.13729	0.00181	861	31	838	15	829	10
16	42	250	35	0.17	0.06121	0.00264	1.14444	0.04884	0.13560	0.00198	647	66	775	23	820	11
17	22	157	22	0.14	0.06568	0.00341	1.23742	0.06296	0.13664	0.00241	796	77	818	29	826	14
18	92	298	45	0.31	0.06308	0.00128	1.20221	0.02479	0.13824	0.00173	711	24	802	11	835	10
19	26	189	28	0.14	0.06689	0.00173	1.25565	0.03243	0.13615	0.00181	834	32	826	15	823	10
20	22	160	22	0.14	0.05727	0.00191	1.09006	0.03613	0.13806	0.00188	502	49	749	18	834	11

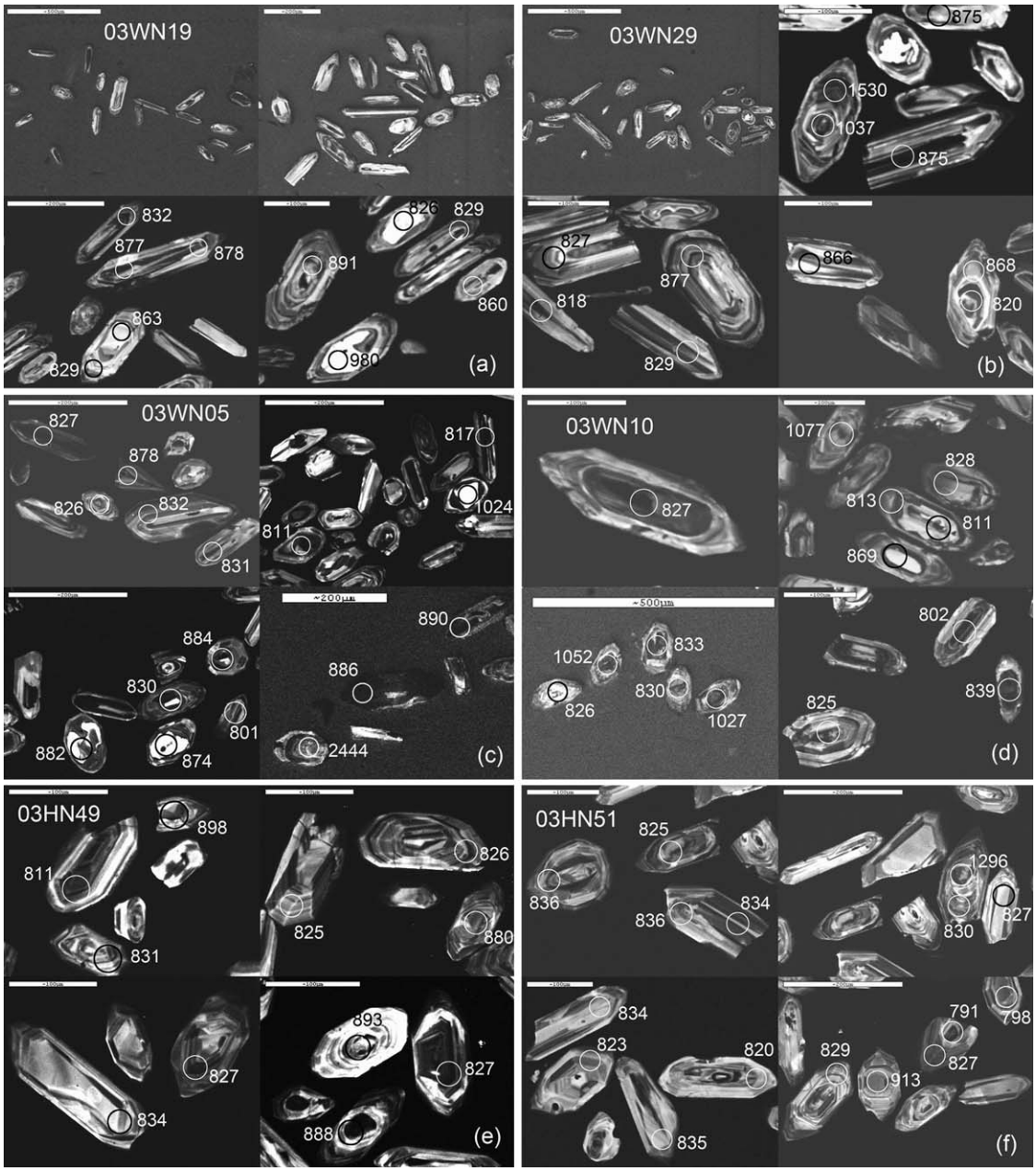

Fig. 2. CL images with $^{206}Pb/^{238}U$ ages (in Ma) for zircons from Neoproterozoic granodiorites in South Anhui: (a) Xucun 03WN19, (b) Xucun 03WN29, (c) Shexian 03WN05, (d) Shexian 03WN10, (e) Xiuning 03HN49, and (f) Xiuning 03HN51.

ent types of Pb/U differentiation in magmatic processes, involving not only Pb loss or U gain but also Pb gain or U loss in a common system (Zheng, 1990, 1992; Ludwig, 1998).

4.1.1. Xucun

Zircons from the Xucun pluton are euhedral, transparent, and colorless. Most of them are short to long prismatic and their lengths range from 100 to 300 μm, with ratios of length to width ranging from 1.5:1 to 6:1. In CL image (Fig. 2a and b), most zircons have homogeneous planar or oscillatory zoning, which is typical for magmatic zircon. Some crystals exhibit structures of core-rim, core-mantle or core-mantle-rim. The cores are unzoned with strong luminescence or are oscillatory zoned with medium CL brightness, and show clear resorption structure (Fig. 2a). They are considered to represent inherited domains that have been modified

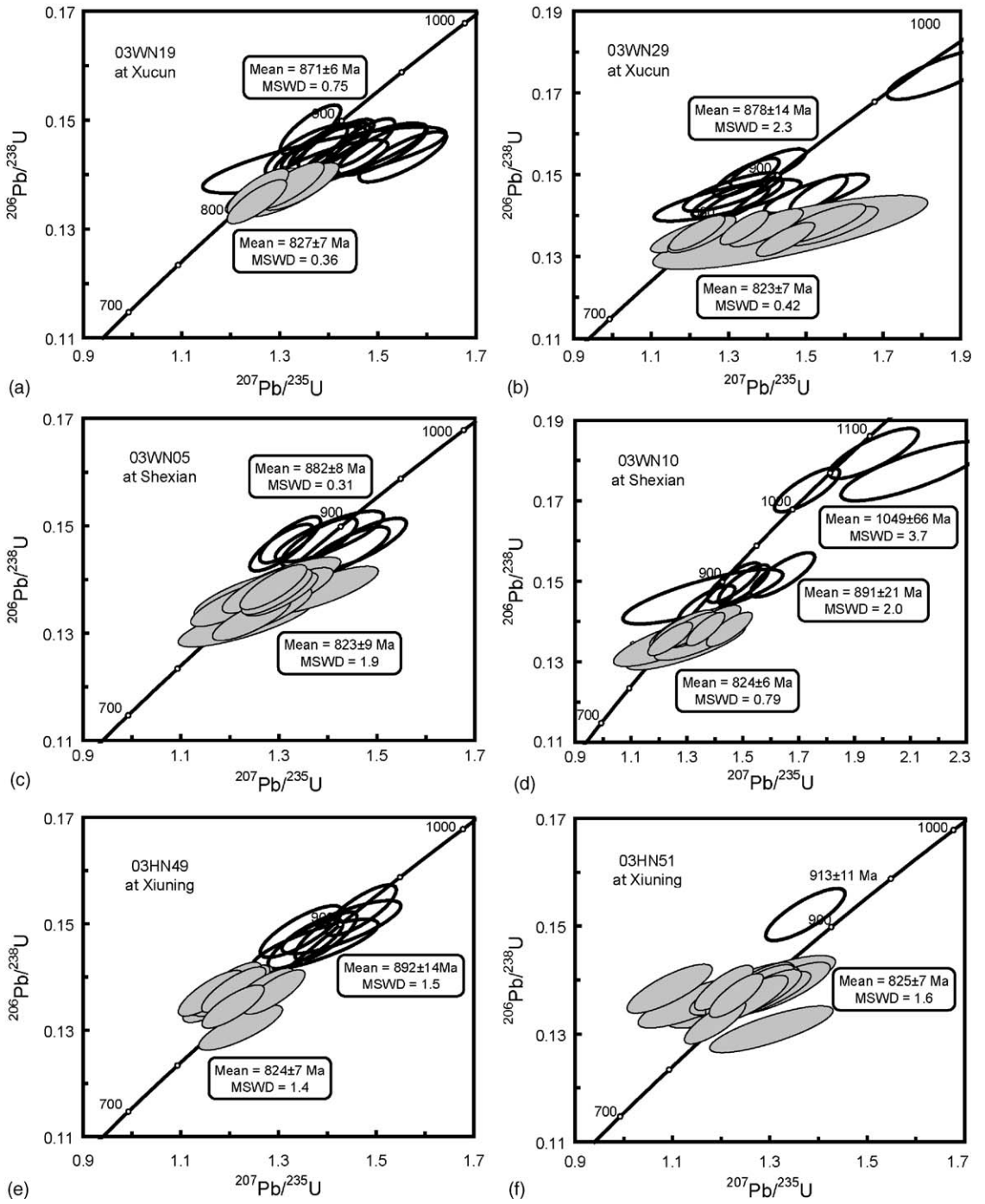

Fig. 3. Zircon U–Pb concordia diagrams for Neoproterozoic granodiorites in South Anhui. A weighted mean was calculated for each group of $^{206}Pb/^{238}U$ ages: (a) Xucun 03WN19, (b) Xucun 03WN29, (c) Shexian 03WN05, (d) Shexian 03WN10, (e) Xiuning 03HN49, and (f) Xiuning 03HN51.

by recrystallization. The mantles and rims are of variable width and have oscillatory zoning with euhedral shape, and are interpreted as the result of magmatic growth.

Sample 03WN19 has U contents from 95 to 422 ppm and Th from 31 to 241 ppm, with Th/U ratios of 0.12–0.95 (Table 1). Spot #2, a zircon core that has been resorbed and recrystallized, is bright in CL and

yields a $^{206}Pb/^{238}U$ age of 980 ± 13 Ma (Fig. 2a). The other $^{206}Pb/^{238}U$ ages are divided into two groups with weighted means at 871 ± 6 and 827 ± 7 Ma, respectively (Fig. 3a). From their CL images, Th and U contents and Th/U ratios, there is no apparent discrimination between the two age groups of zircon. Thus both are of magmatic origin. Nevertheless, most of the old ages are found in the zircon cores (Fig. 2a), and many of them just have narrow rims of magmatic growth that truncate the internal domains of magmatic zoning.

Sample 03WN29 has U contents from 167 to 494 ppm and Th from 26 to 226 ppm with Th/U ratios of 0.13–0.68 (Table 1), but one analysis has a ratio of 0.07 due to its relatively high U content of 494 ppm. Spots #4 and #5 were located in the core and mantle of the same zircon, and are truncated by magmatic growth banding in the rim (Fig. 2b). The mantle preserves magmatic zoning and yields a $^{206}Pb/^{238}U$ age of 868 ± 11 Ma. The core is dark and unzoned due to recrystallization, giving a $^{206}Pb/^{238}U$ age of 820 ± 10 Ma that is much younger than the mantle age. The cores must actually be older and it is the accumulation of radiation damage that made them easily recrystallize and reset their U–Pb systems to produce the younger ages. A similar phenomenon occurs in a zircon with spots #11 and #12 that give a $^{206}Pb/^{238}U$ age of 1530 ± 16 Ma for the mantle (#12) and 1037 ± 14 Ma for the core (#11). The other $^{206}Pb/^{238}U$ ages form two groups, with weighted means at 878 ± 14 and 823 ± 7 Ma, respectively (Fig. 3b). Except for the grain containing spots #4 and #5, the old ages are usually found in the zircon cores (Fig. 2b).

4.1.2. Shexian

Zircons from the Shexian pluton are subhedral to euhedral, transparent, colorless to light yellow. Most of them are equant to long prismatic. Crystals range in length from 80 to 200 μm, with ratios of length to width ranging from 1:1 to 4:1. CL imaging reveals that most zircons are homogeneously oscillatory or planar zoned (Fig. 2c and d), and are interpreted as the result of magmatic growth. Some grains have core-rim structure. The cores are unzoned or weakly zoned with resorption structures, and represent inherited domains. The rims exhibit distinct oscillatory or planar zoning with an euhedral shape, and are interpreted as magmatic zircon. A few crystals have weakly zoned or convoluted zonal features, indicating that the whole grain may be inherited.

Sample 03WN05 has U contents from 122 to 420 ppm and Th from 29 to 233 ppm, with Th/U ratios of 0.14–0.86 (Table 1). Spots #7, #11 and #12 are located in cores that are resorbed and recrystallized and show bright luminesence (Fig. 2c) with relatively lower U contents (Table 1). They yield $^{207}Pb/^{206}Pb$ ages of 980 ± 52 to 1062 ± 32 Ma and $^{206}Pb/^{238}U$ ages of 874 ± 10 to 1024 ± 13 Ma. Except for spots #6 and #7 that have $^{206}Pb/^{238}U$ ages of 2444 ± 25 and 1024 ± 13 Ma, the other $^{206}Pb/^{238}U$ ages form two groups with weighted means at 882 ± 8 and 823 ± 9 Ma, respectively (Fig. 3c).

Sample 03WN10 has U contents from 153 to 549 ppm and Th from 43 to 232 ppm, with Th/U ratios of 0.15–0.78 (Table 1). Spots #4, #5 and #13 are from cores and yield $^{207}Pb/^{206}Pb$ ages of 1004 ± 63 to 1344 ± 147 Ma and $^{206}Pb/^{238}U$ ages of 1027 ± 12 to 1077 ± 14 Ma with a weighted mean at 1049 ± 66 Ma (Fig. 3d). The other ages are divided into two groups with weighted means at 891 ± 21 and 824 ± 6 Ma, respectively.

4.1.3. Xiuning

Zircons from the Xiuning pluton are euhedral, translucent and colorless. Most of them are short prismatic and range from 80 to 200 μm in length, and have length to width ratios ranging from 1.5:1 to 4:1. CL images reveal that most grains have homogeneous oscillatory or planar zoning (Fig. 2e and f), typical of magmatic zircon. Some grains have distinctly luminescent cores, and are inherited domains that have experienced different degrees of recrystallization. A few crystals have weakly zoned rims with cloudy transparency and rounded terminations, which usually form in magmatic grains that experienced hydrothermal alteration (Corfu et al., 2003).

Sample 03HN49 has U contents from 177 to 314 ppm and Th from 25 to 130 ppm, with Th/U ratios of 0.12–0.58, with one analysis having a ratio of 0.08 due to its relatively high U content of 314 ppm (Table 1). All $^{206}Pb/^{238}U$ ages are divisible into two groups with weighed means at 892 ± 14 and 824 ± 7 Ma, respectively (Fig. 3e). Most of the old ages are found in the zircon cores (Fig. 2e).

Sample 03HN51 has U contents from 124 to 329 ppm and Th from 19 to 90 ppm, with Th/U ratios of 0.11–0.42 (Table 1). Spots #4 and #14 are inherited cores with $^{207}Pb/^{206}Pb$ ages of 1338 ± 21 to 789 ± 29 Ma and $^{206}Pb/^{238}U$ ages of 1296 ± 15 and 913 ± 11 Ma, respectively. The other $^{206}Pb/^{238}U$ ages are almost consistent with each other, defining a weighted mean of 825 ± 7 Ma (Fig. 3f).

4.1.4. Summary

Collectively, all of the dated zircons from the three plutons have similar U–Pb ages, with the results defining two groups which can be distinguished from their internal structures in the CL images (Fig. 2). In general,

the young zircons are new grains or rims of homogeneous structure with magmatic zoning, whereas most of the old ages occur in cores or as single xenocrysts. The U and Th contents and Th/U ratios indicate that all of the zircons are of magmatic origin (Table 1). The apparent $^{206}Pb/^{238}U$ ages can be divided into three groups: (1) 790–840 Ma are the dominant ages, especially in the Xiuning samples where only a few ages extend beyond this range; it represents the time of magmatic crystallization; (2) 850–940 Ma are less common than the first group but very common in the samples from the Xucun and Shexian plutons, where they commonly occur in cores and are thus interpreted as inherited ages representing an earlier magmatic event; (3) 950–2444 Ma are found rarely and interpreted as inherited ages possibly derived from the source region. Although there are some differences between the zircon U–Pb ages from the different plutons, they are generally consistent within the limit of errors.

The U–Pb ages for the first group of co-magmatic zircon are 824 ± 6 to 815 ± 17 Ma, which can be calculated as a weighted mean at 824 ± 6 Ma (Fig. 4a). This agrees with the SHRIMP zircon U–Pb age of 823 ± 8 Ma for the granodiorite from the Xucun pluton (Li et al., 2003a). The ages for the second group of inherited zircon are 892 ± 14 to 877 ± 9 Ma, with a weighted mean of 882 ± 16 Ma (Fig. 4b). A few U–Pb ages of 1296–2444 Ma are inherited from their source rocks that contain old crustal material of Paleoproterozoic to Mesoproterozoic age.

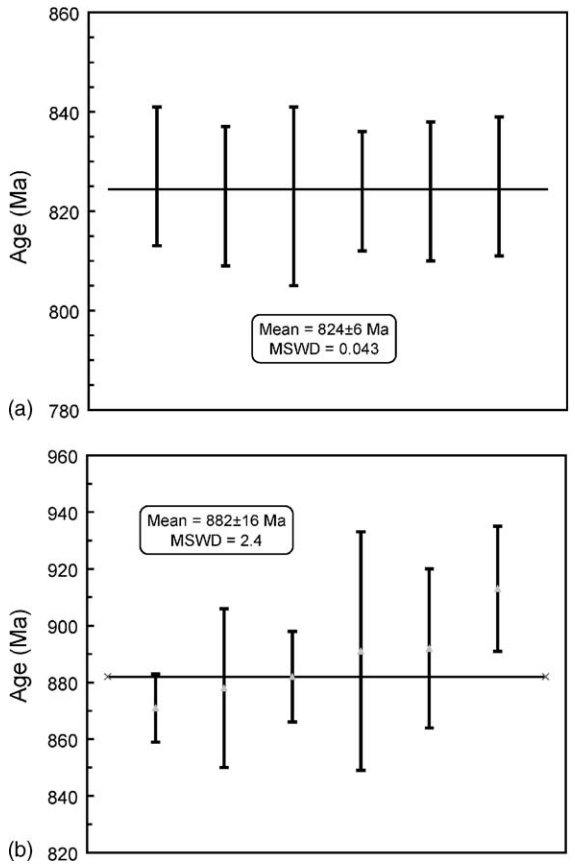

Fig. 4. Diagram of weighted mean U–Pb ages for zircons from Neoproterozoic granodiorites in South Anhui (each bar denotes a single age in Fig. 3): (a) the young group of ages for post-collisional magmatism and (b) the old group of ages for arc-continent collisional magmatism.

4.2. Major and trace elements

Major and trace element data for the granodiorites from South Anhui are presented in Table 2. They have A/CNK ratios of 1.38–1.89 (Table 2), and thus are strongly peraluminous (Sylvester, 1998). In the TAS diagram (Fig. 5), they plot in the granodiorite field. They have variable K_2O contents of 2.8–4.2% with K_2O/Na_2O ratios of 1.2–1.7, CaO of 0.8–1.89 with CaO/Na_2O ratios of 0.29–1.03. They show low Rb contents of 107–151 ppm with low Rb/Sr ratios of 0.48–0.96, relatively high mafic components ($TiO_2 + \Sigma Fe_2O_3 + MgO$) of 3.9–7.4%, but relatively high TiO_2 of 0.29–0.64 with low Al_2O_3/TiO_2 ratios of 23.4–50.8. They have high LOI contents of 1.6–4.1%, suggesting secondary overprinting by various degrees of hydrothermal alteration.

The granodiorites all have similar REE patterns showing LREE-enrichment and moderate negative Eu anomalies ($Eu/Eu^* = 0.43$–0.69) (Fig. 6a). In the primitive mantle-normalized spidergram (Fig. 6b), the granodiorites are characterized by strong enrichment in such

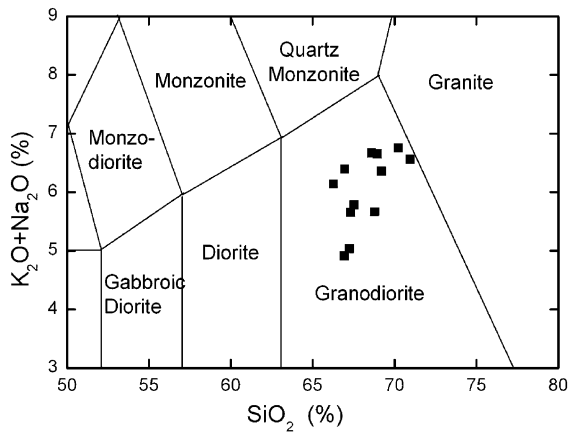

Fig. 5. TAS classification for Neoproterozoic granodiorites in South Anhui (after Middlemost, 1994).

Table 2
Major and trace element compositions of Neoproterozoic granodiorites in South Anhui

Pluton sample	Shexian				Xucun				Xiuning			
	03WN01	03WN05	03WN10	03WN13	03WN15	03WN19	03WN29	03WN31	03WN33	03WN35	03HN49	03HN51
Major element (%)												
SiO_2	67.26	67.33	67.54	68.79	66.28	66.95	69.21	66.93	68.95	68.61	70.24	70.96
TiO_2	0.63	0.54	0.62	0.55	0.63	0.62	0.53	0.64	0.42	0.41	0.34	0.29
Al_2O_3	15.51	15.48	14.92	15.39	15.19	15.17	14.44	14.96	15.63	15.77	15.21	14.73
$(Fe_2O_3)^T$	5.00	4.58	4.93	4.22	4.99	4.52	3.91	4.45	3.28	3.40	2.79	2.63
MnO	0.07	0.07	0.08	0.07	0.09	0.08	0.06	0.07	0.06	0.05	0.05	0.05
MgO	1.73	1.65	1.66	1.34	1.73	1.46	1.35	1.34	1.00	1.24	0.97	1.05
CaO	0.99	1.21	1.42	1.52	1.44	1.38	1.22	1.89	1.36	0.80	0.80	0.97
Na_2O	2.17	2.56	2.21	2.44	2.48	2.57	2.39	1.84	2.47	2.73	2.63	2.88
K_2O	2.86	3.09	3.57	3.22	3.66	3.82	3.96	3.07	4.18	3.93	4.12	3.68
P_2O_5	0.13	0.19	0.17	0.14	0.23	0.16	0.17	0.18	0.21	0.24	0.16	0.19
LOI	3.12	2.77	2.53	1.68	2.72	2.69	2.27	4.04	1.88	2.31	2.20	2.11
Total	99.47	99.47	99.65	99.36	99.44	99.42	99.51	99.41	99.44	99.49	99.51	99.54
A/CNK	1.83	1.59	1.48	1.50	1.40	1.43	1.38	1.53	1.41	1.55	1.49	1.40
Trace element (ppm)												
Mn	513.1	519	593.9	499.1	604.1	560.7	445.5	558.4	413.8	383.7	397.2	419.2
Ni	21.72	21.38	21.63	16.77	18.3	17.94	14.77	18.9	13.07	16.49	10.4	11.82
Ga	18.32	18.03	17.87	17.78	19.68	19.09	17.39	19.46	17.62	19.58	17.46	17.59
Rb	107.8	110.9	117.8	115.1	143.3	144.5	133.2	134.0	133.8	151.0	130.0	132.1
Ba	479.7	580.0	690.6	654.9	575.1	628.1	642.9	469.7	808.3	620.3	894.8	670.9
Th	9.97	8.98	9.15	10.32	11.90	11.63	13.40	11.60	9.31	9.11	8.84	7.07
Nb	10.40	10.52	10.77	10.56	12.51	11.54	11.53	12.51	8.67	9.87	7.17	7.23
Ta	0.82	0.77	0.86	0.82	0.99	0.92	0.93	0.88	0.67	0.72	0.58	0.49
Hf	5.59	4.99	5.43	5.73	6.61	6.55	6.68	6.62	4.58	4.96	4.54	3.72
U	2.80	2.01	2.23	3.83	2.89	2.37	2.87	3.48	2.52	2.52	1.53	1.04
Sr	164.2	185.7	240.8	215.3	163.3	199.5	162.8	140.7	161.0	189.4	196.3	179.0
Zr	191.8	179.6	187.6	184.4	216.7	218.7	224.6	217.1	164.7	186.1	144.9	142.4
Y	29.32	27.56	32.09	29.94	43.21	33.62	34.42	36.52	24.36	33.68	25.64	25.07
La	29.14	27.22	27.52	27.94	31.19	30.13	31.35	30.66	24.49	27.93	24.32	22.45
Ce	60.56	57.54	58.97	59.05	65.7	64.49	67	64.84	51.8	56.85	50.91	47.97
Pr	7.73	7.19	7.34	7.40	8.45	8.05	8.46	8.30	6.73	7.42	6.67	6.01
Nd	29.37	27.07	28.56	28.28	32.49	31.07	32.48	31.7	26.05	28.5	25.51	22.39
Sm	6.18	5.58	6.17	5.90	7.02	6.64	6.85	6.88	5.83	6.27	5.53	4.97
Eu	1.08	1.16	1.17	1.13	1.08	1.10	0.97	1.17	1.00	1.07	1.07	0.89
Gd	5.04	4.72	5.61	5.28	6.77	6.01	6.09	5.96	5.48	5.62	4.97	4.21
Tb	0.86	0.77	0.91	0.90	1.22	1.00	1.03	1.03	0.88	0.92	0.80	0.71
Dy	5.09	4.30	5.40	5.03	7.07	5.60	5.85	6.17	4.53	5.14	4.46	3.69
Ho	1.00	0.84	1.04	0.97	1.37	1.08	1.13	1.16	0.90	0.95	0.89	0.68
Er	2.80	2.44	2.88	2.74	4.12	2.95	2.91	3.22	2.40	2.43	2.38	1.72
Tm	0.46	0.40	0.46	0.43	0.72	0.48	0.50	0.54	0.36	0.39	0.39	0.26
Yb	3.02	2.66	3.03	2.92	4.51	3.02	3.03	3.55	2.44	2.56	2.41	1.65
Lu	0.46	0.39	0.45	0.44	0.72	0.47	0.47	0.52	0.40	0.35	0.39	0.23
Rb/Sr	0.66	0.60	0.49	0.53	0.88	0.72	0.82	0.95	0.83	0.80	0.66	0.74
Eu/Eu*	0.59	0.69	0.61	0.62	0.48	0.53	0.46	0.56	0.54	0.55	0.62	0.60
M[a]	0.82	0.96	1.03	1.00	1.10	1.08	1.07	0.98	1.06	0.97	0.99	1.04
T_{Zr}(°C)[b]	848	831	829	830	838	838	843	847	814	833	808	803

Note: superscripts a and b denote the following equations used for calculation of Zr saturation temperature.

[a] $M = (Na + K + 2Ca)/(Al \times Si)$, after Watson and Harrison (1983).

[b] $T_{Zr} = 12{,}900/[2.95 + 0.85M + \ln(496{,}000/Zr_{melt})]$, after Miller et al. (2003).

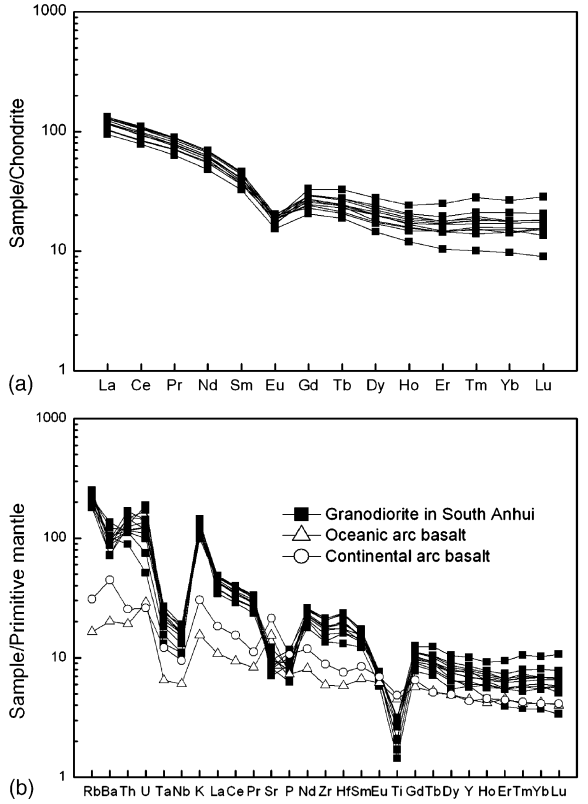

Fig. 6. Normalized patterns of trace element partition for Neoproterozoic granodiorites in South Anhui: (a) chondrite-normalized REE patterns (Chondrite values are from Sun and McDonough, 1989) and (b) primitive mantle-normalized trace element spidergram (primitive mantle values are from McDonough and Sun, 1995). Trace element concentrations of continental arc and oceanic arc basalts are from Kelemen et al. (2003).

large ion lithospheric elements (LILE) as Rb, Ba, Th, U and K, but pronounced negative anomalies in Sr and such high field strength element (HFSE) as Nb, Ta and Ti. This is a common pattern of trace element partition for continental crust that is usually assumed to originate from the geochemical evolution of island arc magmas. When compared with average continental or oceanic arc basalts, similar degrees of the negative Nb and Ta anomalies occur in the granodiorites, but there is much more significant enrichment of LILE (Rb, Ba, U, Th and K) in the granodiorites than in the arc basalts.

According to the CL images and U–Pb dates (Fig. 2), the granodiorites contain inherited zircons and many grains with discrete cores. While the presence of inherited cores suggests incomplete melting of granodioritic magmas, the growth of co-magmatic zircon as discrete grains indicates the saturation of Zr in the melts. As suggested by Miller et al. (2003), for inheritance-rich (>10% grains with premagmatic cores) and inheritance-poor (<10% grains with premagmatic cores) granitoids, T_{Zr} provides a useful estimate and an underestimate of their initial magma temperature, respectively. Therefore, the measured Zr concentration and major element composition of whole-rock can be used to calculate the Zr saturation temperature (T_{Zr}) for granitoids (Watson and Harrison, 1983), which may represent the upper limit of temperatures for zircon crystallization. The calculated T_{Zr} values range from 803 to 848 °C (Table 2 and Fig. 7), with a weighted mean of 829 ± 18 °C. Most of the T_{Zr} values for the Xiuning pluton are lower than the other two plutons (Table 2), mainly because their Zr contents of 142–165 ppm are lower than the others (179–225 ppm).

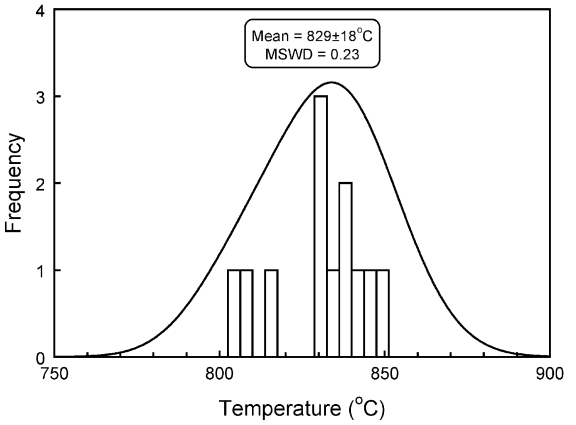

Fig. 7. Histogram of Zr saturation temperatures for Neoproterozoic granodiorites in South Anhui.

4.3. Whole-rock Sr–Nd isotopes

Rb–Sr and Sm–Nd isotopic data for the granodiorites in South Anhui are presented in Table 3. Rb contents range from 107.8 to 151.0 ppm, Sr from 140.7 to 240.8 ppm and $^{87}Rb/^{86}Sr$ ratios vary between 1.413 and 2.755. The small variations in Rb and Sr contents and $^{87}Rb/^{86}Sr$ ratios suggest that the granodioritic magmas were not significantly disturbed by external fluids during their emplacement, crystallization and subsequent evolution by hydrothermal alteration (Zheng, 1989). All the samples have low to medium initial $^{87}Sr/^{86}Sr$ ratios of 0.7033–0.7087 at their emplacement age of 824 Ma. They have relatively constant $^{147}Sm/^{144}Nd$ ratios of 0.124–0.136 and $^{143}Nd/^{144}Nd$ ratios of 0.512158–0.512284. Calculated $\varepsilon_{Nd}(t)$ values are −2.06 to 0.02 at $t = 824$ Ma, and corresponding single-stage Nd model ages (T_{DM1}) are 1.59–1.75 Ga. Because most $^{147}Sm/^{144}Nd$ ratios are greater than 0.13, calculated two-stage Nd model ages (T_{DM2}) cluster at 1.49–1.65 Ga. On an ε_{Nd} versus I_{Sr} diagram (Fig. 8), most of the samples plot below and along the average

Table 3
Rb–Sr and Sm–Nd isotope data for Neoproterozoic granodiorites in South Anhui

Sample	Age (Ma)	Rb (ppm)	Sr (ppm)	$^{87}Rb/^{86}Sr$	$^{87}Sr/^{86}Sr$ ($\pm 2\sigma_m$)	I_{Sr} (t)	Sm (ppm)	Nd (ppm)	$^{147}Sm/^{144}Nd$	$^{143}Nd/^{144}Nd$ ($\pm 2\sigma_m$)	$\varepsilon_{Nd}(t)$	T_{DM1} (Ga)	T_{DM2} (Ga)
Xucun													
03WN15	821	143.3	163.3	2.538	0.735868 ± 13	0.706107	7.02	32.49	0.1307	0.512284 ± 9	0.02	1.59	1.49
03WN19	821	144.5	199.5	2.093	0.729639 ± 15	0.705090	6.64	31.07	0.1292	0.512248 ± 11	−0.52	1.62	1.53
03WN29	821	133.2	162.8	2.366	0.735107 ± 15	0.707362	6.85	32.48	0.1275	0.512243 ± 9	−0.45	1.60	1.52
03WN31	821	134.0	140.7	2.755	0.736692 ± 13	0.704390	6.88	31.7	0.1312	0.512227 ± 8	−1.14	1.70	1.58
Shexian													
03WN01	821	107.8	164.2	1.898	0.730837 ± 12	0.708583	6.18	29.37	0.1272	0.512158 ± 9	−2.06	1.74	1.65
03WN05	821	110.9	185.7	1.726	0.728939 ± 15	0.708700	5.58	27.07	0.1247	0.512182 ± 9	−1.33	1.65	1.60
03WN10	821	117.8	240.8	1.413	0.723918 ± 14	0.707347	6.17	28.56	0.1306	0.512195 ± 9	−1.71	1.75	1.63
03WN13	821	115.1	215.3	1.545	0.726128 ± 13	0.708015	5.90	28.28	0.1262	0.512236 ± 8	−0.43	1.59	1.52
Xiuning													
03WN33	821	133.8	161.0	2.402	0.731561 ± 15	0.703389	5.83	26.05	0.1352	0.512270 ± 9	−0.73	1.71	1.55
03WN35	821	151.0	189.4	2.305	0.733490 ± 16	0.706458	6.27	28.5	0.1331	0.512260 ± 9	−0.70	1.68	1.54
03HN49	821	130.0	196.3	1.914	0.727873 ± 13	0.705431	5.53	25.51	0.1310	0.512254 ± 9	−0.60	1.65	1.54
03HN51	821	132.1	179.0	2.133	0.729493 ± 13	0.704480	4.97	22.39	0.1341	0.512250 ± 10	−1.00	1.72	1.57

Note: the initial Sr and Nd isotope ratios were calculated at $t = 824$ Ma.

Nd isotopic bulk earth line, suggesting their derivation from reworking of evolved juvenile crust and geochemical affinity to I-type granitoid (McCulloch and Chappell, 1982).

4.4. Zircon Hf isotopes

Three samples of zircon that were dated by U–Pb were also analysed for their Lu–Hf isotopes on domains of the same or similar structure, and the results are listed in Table 4. Initial $^{176}Hf/^{177}Hf$ ratios and $\varepsilon_{Hf}(t)$ values were calculated at $t = 824$ Ma (Fig. 4a), which registers the timing of zircon growth from the granodioritic magmas.

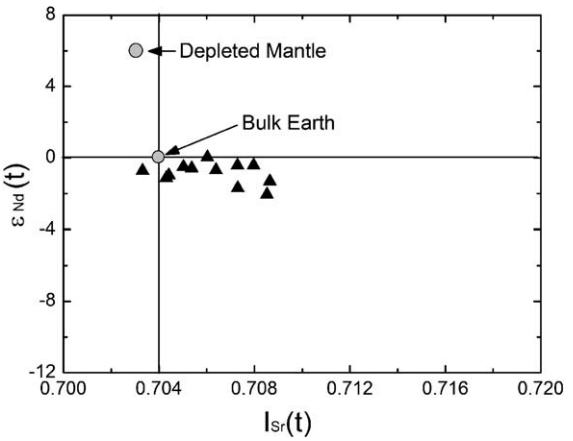

Fig. 8. Diagram of initial Nd and Sr isotope ratios in the space of $\varepsilon_{Nd}(t)$ vs. $I_{Sr}(t)$ at $t = 824$ Ma for Neoproterozoic granodiorites in South Anhui.

Figs. 9 and 10 depict the relationship of $^{206}Pb/^{238}U$ age to $^{176}Lu/^{177}Hf$ and $(^{176}Hf/^{177}Hf)_i$ ratios for the same spots, and Figs. 11 and 12 show histograms of $\varepsilon_{Hf}(t)$ values and Hf model ages for the three samples, respectively.

4.4.1. Xucun

Twenty Lu–Hf spot analyses were made on zircons from sample 03WN29 from the Xucun pluton. No significant difference is observed between $^{206}Pb/^{238}U$ age and $^{176}Lu/^{177}Hf$ ratio (Fig. 9a), but the three oldest U–Pb ages of 1037–1530 Ma (spots #11, #12 and #15 in Table 4) are associated with the lowest $(^{176}Hf/^{177}Hf)_i$ ratios of 0.282238–0.282250 (Fig. 10a) and thus the lowest $\varepsilon_{Hf}(t)$ values of −0.8 to −0.3 (Fig. 11b), indicating the presence of Mesoproterozoic crustal relicts in the source of Neoproterozoic magmatism. All other domains show positive $\varepsilon_{Hf}(t)$ values of 1.6–9.9, with a weighted mean of 5.4 ± 2.6 (Fig. 11a). Correspondingly, their Hf model ages are 989–1319 Ma, with a weighted mean of 1.17 ± 0.08 Ga (Fig. 12a). The highest $(^{176}Hf/^{177}Hf)_i$ ratio of 0.282537 occurs in an inherited domain with a $^{206}Pb/^{238}U$ age of 877 ± 11 Ma, corresponding to the maximum $\varepsilon_{Hf}(t)$ value of 9.9 and the youngest T_{DM} age of 989 Ma. This may indicate the incorporation of a juvenile component during protolith magmatism at ca. 880 Ma and thus a significant contribution of depleted mantle to its source.

Three grains with core-rim structure were measured for both U–Pb and Lu–Hf isotopes (Table 4 and Fig. 13). One grain) with two U–Pb ages of 820 ± 10 and 868 ± 11 Ma shows different $\varepsilon_{Hf}(t)$ values of 1.6

Table 4
LA-MC-ICPMS Zircon Lu–Hf isotope data for Neoproterozoic granodiorites in South Anhui

Spot no.	$^{176}Yb/^{177}Hf$	$^{176}Lu/^{177}Hf$	$^{176}Hf/^{177}Hf$	$\pm(2\sigma)$	Age (Ma)	$(^{176}Hf/^{177}Hf)_i$	$\varepsilon_{Hf}(t)$	$\pm(2\sigma)$	T_{DM} (Ma)	$\pm(2\sigma)$
03WN29 (Xucun)										
1	0.024364	0.001204	0.282557	0.000030	877 ± 11	0.282539	9.9	0.5	989	42
2	0.038822	0.001665	0.282433	0.000027	827 ± 10	0.282407	5.2	0.5	1180	39
3	0.037031	0.001603	0.282465	0.000036	818 ± 10	0.282440	6.4	0.6	1132	51
5	0.039407	0.001798	0.282419	0.000043	868 ± 11	0.282391	4.7	0.8	1204	62
4	0.026191	0.001155	0.282322	0.000036	820 ± 10	0.282304	1.6	0.7	1319	51
6	0.029654	0.001287	0.282542	0.000046	866 ± 12	0.282523	9.3	0.8	1013	65
7	0.038931	0.001701	0.282391	0.000033	861 ± 10	0.282365	3.7	0.6	1240	48
8	0.040716	0.001786	0.282394	0.000045	910 ± 11	0.282367	3.8	0.8	1239	64
9	0.032119	0.001287	0.282411	0.000041	897 ± 11	0.282391	4.7	0.7	1198	58
10	0.035020	0.001551	0.282461	0.000036	821 ± 21	0.282437	6.3	0.6	1136	51
11	0.033519	0.001532	0.282262	0.000027	1037 ± 14	0.282238	−0.8	0.5	1419	39
12	0.032187	0.001486	0.282273	0.000042	1530 ± 16	0.282250	−0.3	0.8	1400	59
13	0.038375	0.001582	0.282435	0.000032	875 ± 10	0.282410	5.3	0.6	1174	46
14	0.026888	0.001201	0.282349	0.000046	875 ± 11	0.282331	2.5	0.8	1283	65
15	0.043717	0.001968	0.282276	0.000047	1287 ± 14	0.282245	−0.5	0.9	1415	68
16	0.043661	0.001889	0.282373	0.000046	829 ± 11	0.282344	3.0	0.8	1273	66
17	0.025494	0.001127	0.282510	0.000046	811 ± 10	0.282493	8.3	0.8	1054	65
18	0.029705	0.001291	0.282489	0.000036	833 ± 11	0.282469	7.4	0.7	1089	51
19	0.037496	0.001650	0.282422	0.000051	818 ± 11	0.282396	4.8	0.9	1195	73
20	0.008740	0.000377	0.282324	0.000042	827 ± 11	0.282318	2.1	0.8	1291	58
03WN05 (Shexian)										
1	0.031406	0.001466	0.282346	0.000025	832 ± 10	0.282324	2.3	0.4	1296	35
2	0.044931	0.002037	0.282406	0.000048	827 ± 9	0.282375	4.1	0.9	1230	69
3	0.018424	0.000827	0.282299	0.000048	831 ± 10	0.282286	0.9	0.9	1340	67
5	0.067467	0.002956	0.282408	0.000061	890 ± 11	0.282363	3.6	1.1	1258	90
4	0.044007	0.002030	0.282391	0.000030	886 ± 10	0.282360	3.5	0.5	1252	43
6	0.011770	0.000534	0.281468	0.000040	2444 ± 25	0.281459	-28.4	0.7	2466	54
7	0.018862	0.000819	0.282309	0.000028	1024 ± 13	0.282297	1.3	0.5	1325	39
8	0.028696	0.001268	0.282446	0.000058	817 ± 10	0.282426	5.9	1.1	1149	82
9	0.014608	0.000610	0.282329	0.000062	811 ± 10	0.282320	2.1	1.1	1291	86
10	0.032893	0.001459	0.282362	0.000048	801 ± 9	0.282339	2.8	0.9	1274	68
11	0.022998	0.001048	0.282476	0.000057	874 ± 10	0.282460	7.1	1.0	1100	80
12	0.027814	0.001342	0.282405	0.000033	882 ± 11	0.282384	4.4	0.6	1209	47
13	0.033694	0.001515	0.282435	0.000039	841 ± 10	0.282412	5.4	0.7	1172	56
14	0.028826	0.001322	0.282364	0.000034	830 ± 10	0.282344	3.0	0.6	1266	49
15	0.014928	0.000734	0.282314	0.000026	884 ± 10	0.282303	1.5	0.5	1315	36
16	0.017119	0.000757	0.282389	0.000023	835 ± 10	0.282377	4.2	0.4	1213	32
17	0.054596	0.002370	0.282473	0.000038	832 ± 10	0.282437	6.3	0.7	1144	56
18	0.023878	0.001021	0.282427	0.000042	798 ± 11	0.282412	5.4	0.8	1167	59
19	0.048448	0.002148	0.282435	0.000047	878 ± 10	0.282402	5.0	0.8	1192	68
03HN49 (Xiuning)										
1	0.021568	0.000918	0.282406	0.000028	788 ± 10	0.282392	4.7	0.5	1194	39
2	0.018335	0.000776	0.282406	0.000036	880 ± 11	0.282394	4.8	0.7	1190	51
3	0.024121	0.001059	0.282335	0.000029	826 ± 10	0.282318	2.1	0.5	1298	41
5	0.020498	0.000895	0.282407	0.000026	825 ± 10	0.282393	4.7	0.5	1192	36
4	0.025215	0.001102	0.282349	0.000026	828 ± 10	0.282332	2.6	0.5	1280	36
6	0.047053	0.001968	0.282379	0.000027	827 ± 10	0.282349	3.1	0.5	1267	39
7	0.013393	0.000556	0.282382	0.000023	893 ± 11	0.282373	4.0	0.4	1216	32
8	0.076423	0.003099	0.282385	0.000031	879 ± 11	0.282338	2.8	0.6	1297	46
9	0.046187	0.002048	0.282388	0.000039	888 ± 10	0.282357	3.4	0.7	1256	56
10	0.036908	0.001575	0.282422	0.000027	825 ± 10	0.282398	4.9	0.5	1192	38
11	0.016260	0.000695	0.282353	0.000024	811 ± 10	0.282342	2.9	0.4	1261	33
12	0.075570	0.003258	0.282374	0.000036	898 ± 11	0.282324	2.3	0.7	1320	54
13	0.020017	0.000870	0.282376	0.000025	831 ± 10	0.282363	3.6	0.5	1234	35

Table 4 (*Continued*)

Spot no.	$^{176}Yb/^{177}Hf$	$^{176}Lu/^{177}Hf$	$^{176}Hf/^{177}Hf$	$\pm(2\sigma)$	Age (Ma)	$(^{176}Hf/^{177}Hf)_i$	$\varepsilon_{Hf}(t)$	$\pm(2\sigma)$	T_{DM} (Ma)	$\pm(2\sigma)$
14	0.018596	0.000853	0.282318	0.000024	819 ± 10	0.282305	1.6	0.4	1315	33
15	0.028895	0.001217	0.282424	0.000031	829 ± 11	0.282405	5.1	0.6	1178	43
16	0.028037	0.001208	0.282400	0.000027	915 ± 11	0.282381	4.3	0.5	1212	38
17	0.020430	0.000888	0.282366	0.000027	829 ± 10	0.282353	3.3	0.5	1248	38
18	0.040762	0.001764	0.282406	0.000033	831 ± 10	0.282379	4.2	0.6	1221	48
19	0.024197	0.001063	0.282362	0.000023	834 ± 10	0.282346	3.0	0.4	1260	33
20	0.029408	0.001323	0.282382	0.000021	827 ± 10	0.282361	3.6	0.4	1241	30

Note: spot number is the same as that for LA-ICPMS U–Pb dating, and age denotes the $^{206}Pb/^{238}U$ age; the initial Hf isotope ratios were calculated at $t = 824$ Ma.

and 4.7, respectively (Fig. 13a). Clearly, they reflect two different types of domain; the young core with the low $\varepsilon_{Hf}(t)$ value indicates incorporation of a crustal component by fluid/melt infiltration during partial melting to cause anatectic recrystallization. In contrast, one grain with the indistinguishable U–Pb ages of 811 ± 10 and 833 ± 11 Ma gives the similar $\varepsilon_{Hf}(t)$ values of 8.3 and 7.4 (Fig. 13c), responsible for the two domains of the same origin during zircon growth from the granodioritic magma. Nevertheless, the inherited zircon with two older U–Pb ages of 1530 ± 16 and 1037 ± 14 Ma yields consistently negative $\varepsilon_{Hf}(t)$ values of −0.3 and −0.8, respectively (Fig. 13b).

4.4.2. Shexian

Nineteen Lu–Hf spot analyses were made on zircons from sample 03WN05 from the Shexian pluton. There is also no significant difference between $^{206}Pb/^{238}U$ age and $^{176}Lu/^{177}Hf$ ratio (Fig. 9b). As listed in Table 1, the lowest $(^{176}Hf/^{177}Hf)_i$ ratio of 0.281459 is associated with the oldest U–Pb concordant ages of 2425 ± 11 to 2444 ± 25 Ma. Correspondingly, a strongly negative $\varepsilon_{Hf}(t)$ value of −28.4 is obtained, with the oldest T_{DM} age of 2466 ± 54 Ma (spot #6 in Table 4). Consistency between the U–Pb and Hf model ages suggests magma extraction from the depleted mantle at about 2.45 Ga for the oldest crustal relict, which was then incorporated into the source of Neoproterozoic granodiorites. Except for this grain, $\varepsilon_{Hf}(t)$ values scatter between 0.9 and 7.1, with a weighted mean of 3.4 ± 1.6 (Fig. 11b). Correspondingly, their Hf model ages are 1100–1340 Ma with a weighted mean of 1.25 ± 0.06 Ga (Fig. 12b). The highest $(^{176}Hf/^{177}Hf)_i$ ratio of 0.282460 occurs in an inherited grain with a U–Pb age of 874 ± 10 Ma, corresponding to the maximum $\varepsilon_{Hf}(t)$ value of 7.1 and the youngest T_{DM} age of 1100 Ma. This may suggest the incorporation of an evolved juvenile component during protolith magmatism at ca. 880 Ma and thus a contribution of depleted mantle to its protolith source.

4.4.3. Xiuning

Twenty Lu–Hf spot analyses were made on zircons from sample 03HN49 from the Xiuning pluton. Although no correlation is observed between $^{206}Pb/^{238}U$ age and $^{176}Lu/^{177}Hf$ ratio (Fig. 9c), the two highest $^{176}Lu/^{177}Hf$ ratios of 0.003099–0.003258 are associated with inherited grains with U–Pb ages of 879 ± 11 to 898 ± 11 Ma (Table 4). Uniformly positive $\varepsilon_{Hf}(t)$ values of 1.6–5.1 were obtained with a weighted mean of 3.5 ± 0.9 (Fig. 11c). Correspondingly, their Hf model ages are 1178–1315 Ma with a weighted mean of 1.24 ± 0.04 Ga (Fig. 12c).

4.5. Mineral O isotope

Oxygen isotope data for mineral separates from the granodiorites in South Anhui are presented in Table 5. Calculated O isotopic temperatures for quartz-mineral pairs are listed in Table 6. Measured whole-rock $\delta^{18}O$ values cannot reflect the primary $\delta^{18}O$ values because the granodiorites experienced various degrees of post-magmatic alteration. The whole-rock $\delta^{18}O$ values for magma are estimated according to the measured quartz $\delta^{18}O$ values at the temperatures of 750–850 °C using appropriate quartz-granodiorite fractionation factors (Zhao and Zheng, 2003). All the samples plot in the field of S-type granitoids (Fig. 14), consistent with the division of I-type and S-type granitoids by their $\delta^{18}O$ values (O'Neil and Chappell, 1977).

Zircon, quartz and garnet are relatively refractory minerals to O isotope exchange, with small variations in $\delta^{18}O$ values of 8.1–10.2‰, 11.9–14.0‰ and 9.1–10.8‰, respectively (Table 5). In contrast, K-feldspar, plagioclase, biotite and cordierite are also magmatic minerals, but with large variations in $\delta^{18}O$ values of 4.5–11.6‰, 5.6–10.9‰, 4.2–6.5‰ and 4.2–9.2‰, respectively. O isotopic temperatures for these quartz-mineral pairs are lower than 400 °C (Table 6 and Fig. 15a–d), implying these minerals underwent different degrees of post-

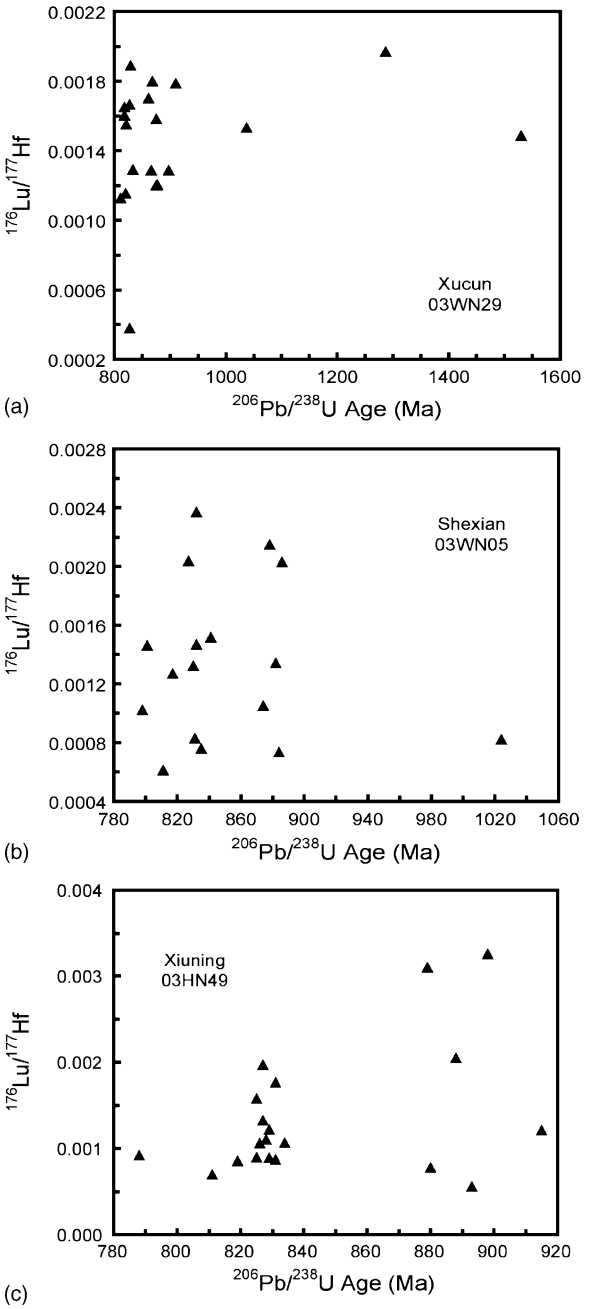

Fig. 9. Relationship between zircon U–Pb age and Lu/Hf ratio for Neoproterozoic granodiorites in South Anhui: (a) Xucun 03WN29, (b) Shexian 03WN05, and (c) Xiuning 03HN49.

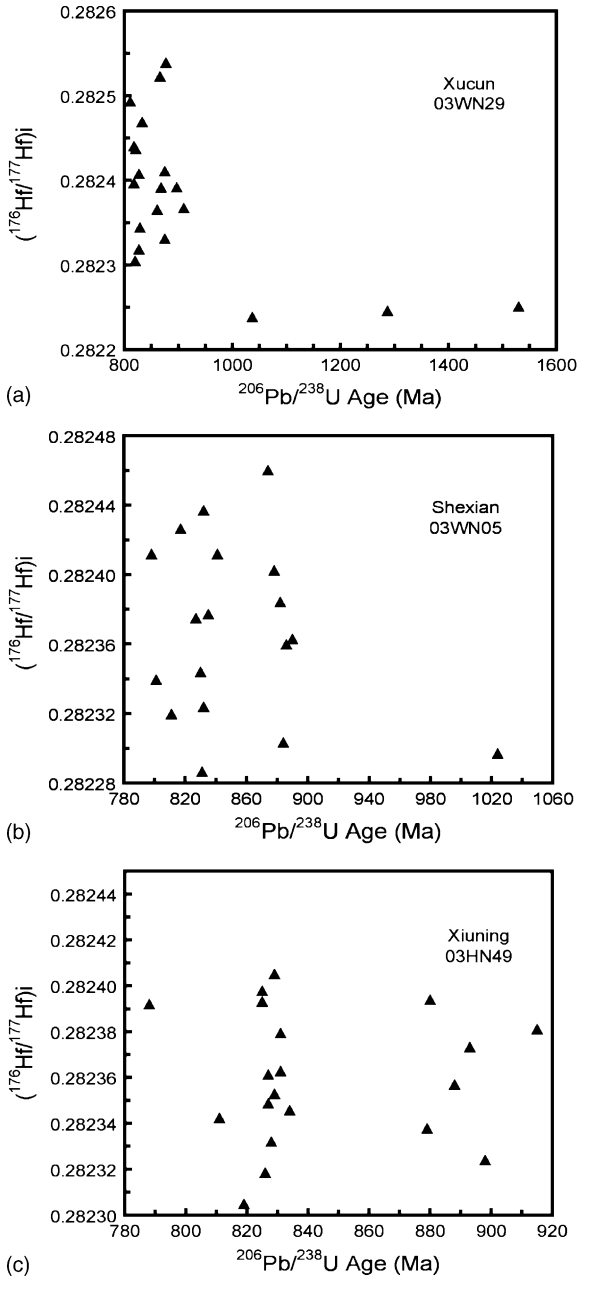

Fig. 10. Relationship between zircon U–Pb age and initial $^{176}Hf/^{177}Hf$ ratio at $t = 824$ Ma for Neoproterozoic granodiorites in South Anhui: (a) Xucun 03WN29, (b) Shexian 03WN05, and (c) Xiuning 03HN49.

magmatic hydrothermal alteration at subsolidus temperatures.

O isotopic temperatures of 500–800 °C were calculated for quartz–zircon pairs (Table 6 and Fig. 15e) with a weighted mean of 601 ± 22 °C (Fig. 16a); 600–850 °C for quartz-garnet pairs (Table 6 and Fig. 15f) with a weighted mean of 750 ± 34 °C (Fig. 16b). These indicate preservation of high-T O isotope equilibria between the relatively refractory minerals. However, the zircon $\delta^{18}O$ values are lower than those for coexisting garnet (Fig. 17), suggesting O isotope disequilibrium between them. The zircon $\delta^{18}O$ values of 8.1–10.2‰ are significantly higher than 5.3 ± 0.3‰ for the normal mantle zircon (Valley et al., 1998), pointing to a secondary magma with high $\delta^{18}O$ values. Although

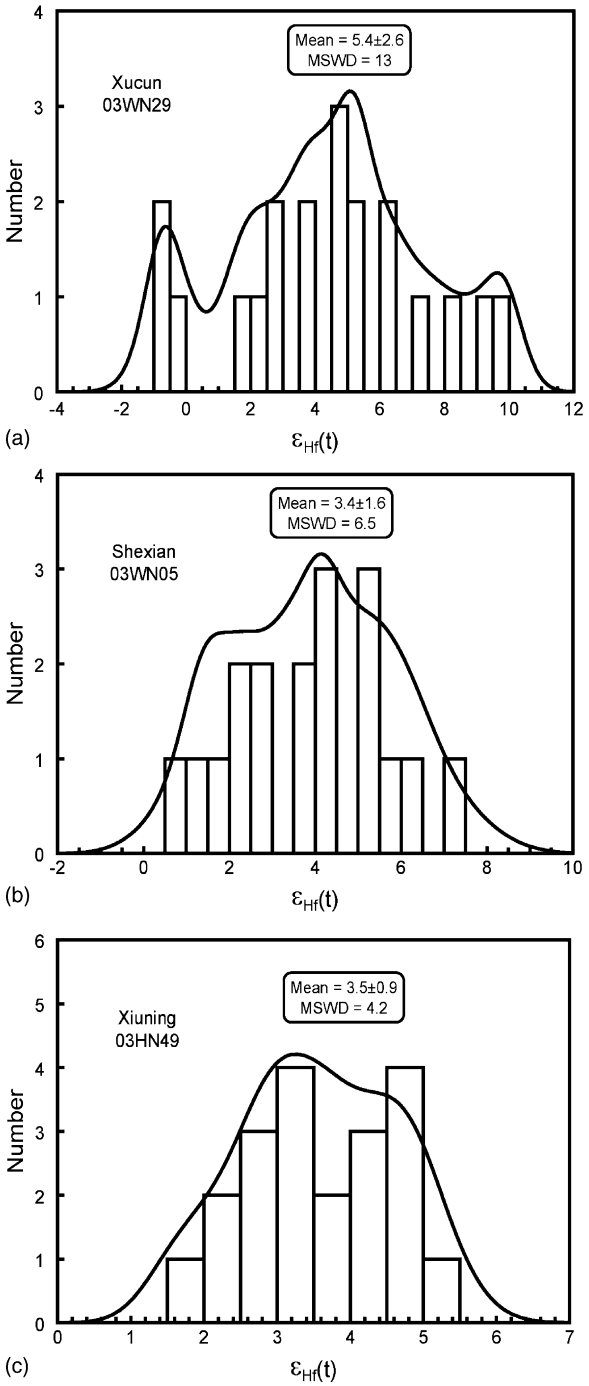

Fig. 11. Histogram of initial Hf isotope composition at $t = 824$ Ma for Neoproterozoic granodiorites in South Anhui: (a) Xucun 03WN29, (b) Shexian 03WN05 [a extremely negative $\varepsilon_{Hf}(t)$ value of -28.4 ± 0.7 is not plotted], and (c) Xiuning 03HN49.

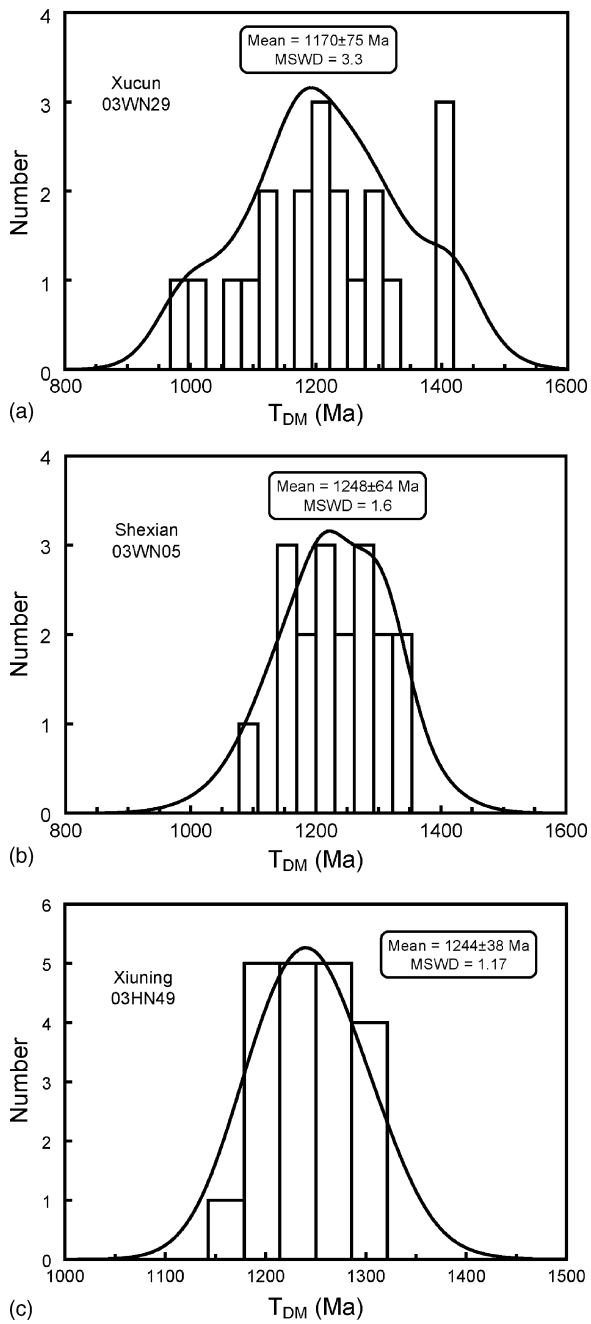

Fig. 12. Histogram of Hf model age for Neoproterozoic granodiorites in South Anhui: (a) Xucun 03WN29, (b) Shexian 03WN05 [a Paleoproterozoic T_{DM} age of 2466 ± 54 Ma is not plotted], and (c) Xiuning 03HN49.

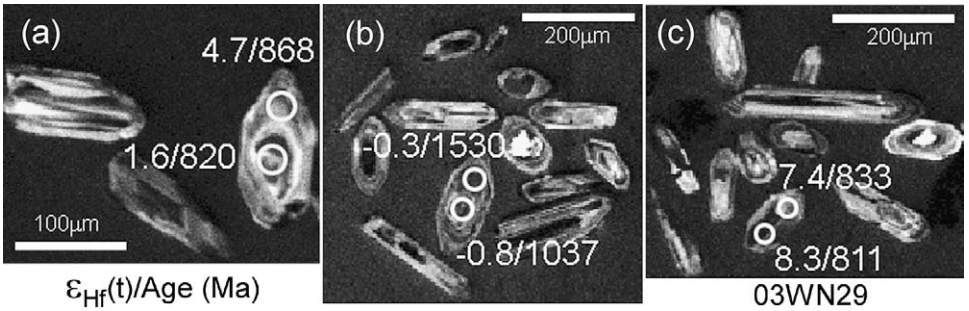

Fig. 13. CL images with both $\varepsilon_{Hf}(t)$ value and U–Pb age for three grains of zircon from granodiorite 03WN29 at Xucun: (a) core and rim have different Neoproterozoic U–Pb ages and Hf isotope ratios, (b) core and rim have older Mesoproterozoic U–Pb ages and lower Hf isotope ratios, and (c) core-rim with similar Neoproterozoic U–Pb ages and Hf isotope ratios.

metamict zircon is susceptible to post-magmatic subsolidus hydrothermal alteration due to radiation damage (Geisler et al., 2001, 2002), crystalline zircon is resistant to subsolidus water–rock interaction and dry granulite-facies metamorphism and thus capable of preserving its magmatic $\delta^{18}O$ value (Valley, 2003; Zheng et al., 2004). Therefore, the high-^{18}O magma is derived from the remelting of a crustal source that experienced significant chemical weathering rather than directly from a mantle source.

Muscovite and chlorite are secondary minerals with the $\delta^{18}O$ values of 4.3–10.7‰ and 0.5–6.7‰, respectively (Table 5). Most O isotopic temperatures for quartz-muscovite pairs vary between 400 and 600 °C (Table 6 and Fig. 15g), indicating O isotope reequilibration at medium temperatures. Most temperatures for quartz-chlorite pairs vary between 150 and 300 °C (Table 6 and Fig. 15h), suggesting secondary alteration at low temperatures.

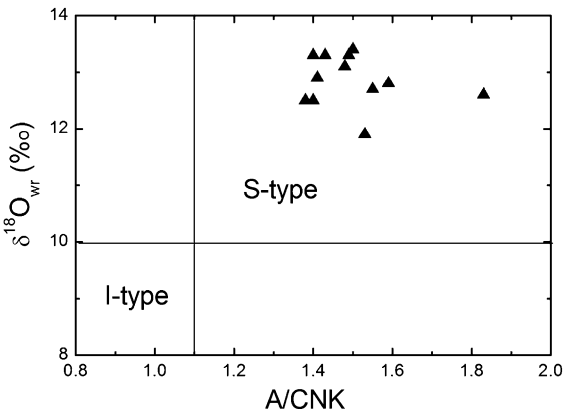

Fig. 14. Diagram of $\delta^{18}O$ vs. A/CNK for Neoproterozoic granodiorites in South Anhui. $\delta^{18}O$ values and A/CNK ratios for I- and S-type granites are from O'Neil and Chappell (1977) and Chappell and White (2001).

5. Discussion

5.1. Petrogenesis of the granodiorites

The present study shows that the granodiorites in South Anhui share many features in terms of element and isotope geochemistry with the metasedimentary rocks of the adjacent Shangxi Group, particularly in the arc-like patterns of REE and trace element partition (Xing et al., 1988), as well as initial Nd isotope ratios and Nd model ages (Chen and Jahn, 1998). This suggests a genetic connection with respect to their protolith origin in an island arc setting. Most $^{206}Pb/^{238}U$ ages for inherited zircons from the granodiorites in South Anhui spread between 913 ± 11 and 877 ± 9 Ma (Table 7), with a cluster at 882 ± 16 Ma (Fig. 4b). This is consistent with TIMS multi-grain $^{207}Pb/^{206}Pb$ ages of 904 ± 4 to 875 ± 4 Ma for arc-like volcanic rocks from the Shuangxiwu Group in the northern part of Zhejiang province (Cheng, 1993). Thus occurrence of extensive magmatism at ca. 900 ± 20 Ma is evident between the Yangtze and Cathaysia Blocks. The igneous rocks in North Zhejiang with ages of ca. 910–870 Ma are also characterized by positive $\varepsilon_{Nd}(t)$ values of 3.0–6.2, low $I_{Sr}(t)$ values of 0.7023–0.7043, and mantle-like $\delta^{18}O$ values of 5.7–6.7‰ (Shen et al., 1999), implying an origin from mantle-derived magma.

The granodiorites in South Anhui show the features typical of S-type granites, with high A/CNK ratios of 1.3–1.9 (Table 2) and high $\delta^{18}O$ values of 11.94–14.02‰ for quartz and 8.09–10.23‰ for zircon (Table 5). These indicate that their source rocks experienced chemical weathering and thus had a supracrustal origin. High CaO/Na_2O ratios of 0.29–1.03 were obtained from the geochemical analyses (Table 2), suggesting that the sources had a psammatic dominance (Sylvester, 1998). Low-pressure melting is expected to take place

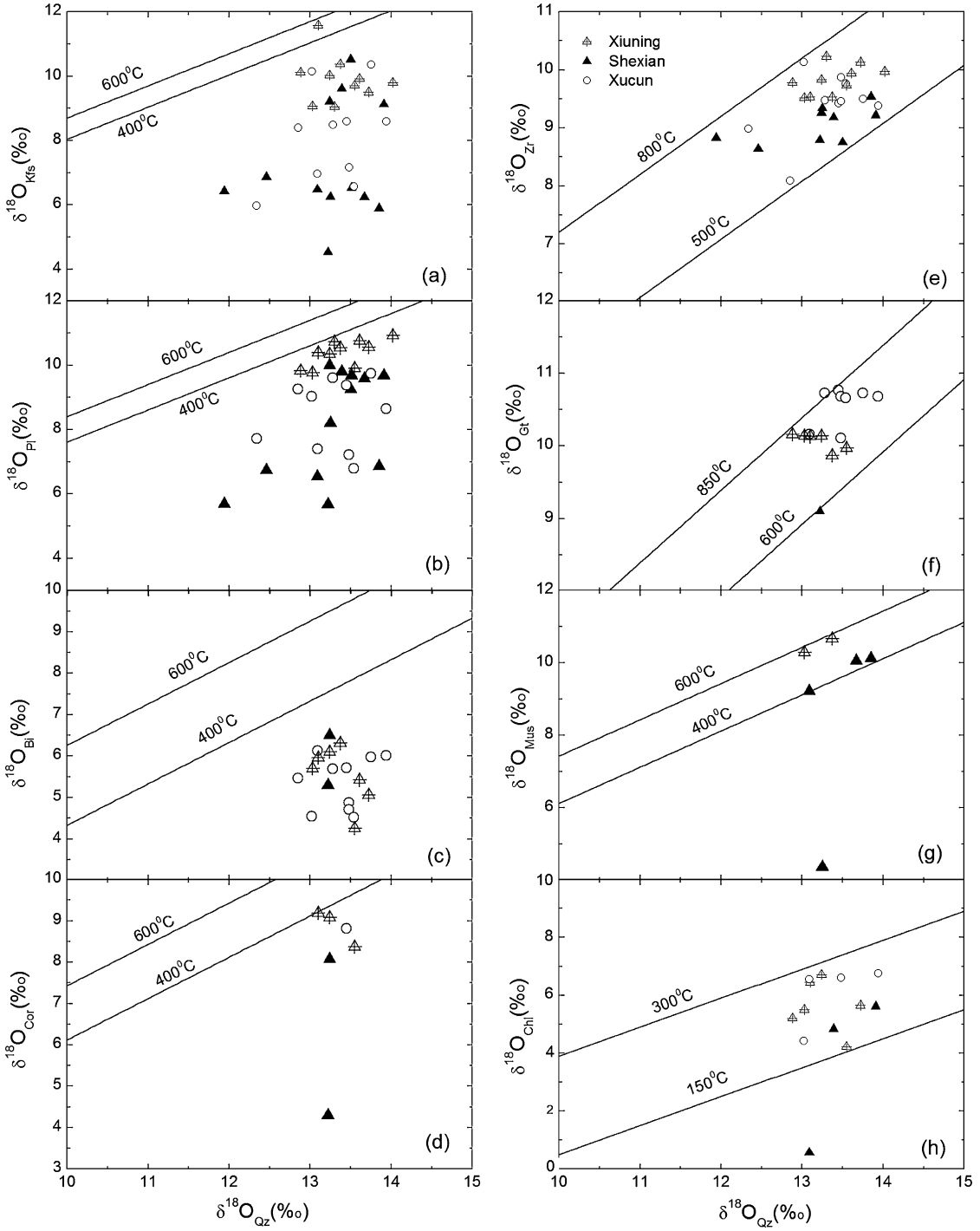

Fig. 15. Plots of quartz $\delta^{18}O$ value vs. other minerals $\delta^{18}O$ values for Neoproterozoic granodiorites in South Anhui: (a) quartz vs. K-feldspar, (b) quartz vs. plagioclase, (c) quartz vs. biotite, (d) quartz vs. cordierite, (e) quartz vs. zircon, (f) quartz vs. garnet, (g) quartz vs. muscovite, (h) quartz vs. chlorite.

Table 5
Oxygen isotope composition of mineral separates from granodiorites in South Anhui ($\delta^{18}O$ in permil relative to VSMOW)

Sample	WR	Qz	Zr	Gt	Pl	Kfs	Bi	Cor	Ilm	Mus	Chl
Xucun											
03WN15	13.1–13.5	13.94	9.38	10.68	8.65	8.59	6.01				6.75
03WN16	13.0–13.4	13.75	9.50	10.73	9.75	10.36	5.98				
03WN17	11.5–11.9	12.34	8.98		7.72	5.98					
03WN18	12.6–13.0	13.45	9.42	10.77	9.37	8.59	5.71	8.81			
03WN19	12.7–13.1	13.48	9.25	10.11	7.21	7.16	4.87				6.61
03WN27	12.7–13.1	13.48	9.46	10.68			4.71				
03WN28	12.7–13.1	13.54	9.76	10.66	6.79	6.57	4.52				
03WN29	12.5–12.9	13.28	9.47	10.73	9.61	8.48	5.69				
03WN30	12.1–12.5	12.85	8.09		9.25	8.39	5.47				
03WN31	12.3–12.7	13.09		10.16	7.40	6.97	6.13				6.55
03WN32	12.2–12.6	13.02	10.13		9.02	10.15	4.54				4.42
Shexian											
03WN01	12.3–12.7	13.09			6.53	6.48				9.22	0.57
03WN02	12.9–13.3	13.67			9.59	6.24				10.06	
03WN03	12.7–13.1	13.51			9.68	6.53					
03WN04	12.4–12.8	13.25	9.34		8.20	6.25				4.36	
03WN05	13.1–13.5	13.85	9.54		6.85	5.89				10.12	
03WN06	12.4–12.8	13.22	8.79	9.10	5.67	4.53	5.29	4.29			
03WN09	12.6–13.0	13.39	9.18		9.79	9.62					4.84
03WN10	13.1–13.5	13.91	9.22		9.68	9.13					5.62
03WN11	12.4–12.8	13.24	9.26		10.00	9.21	6.50	8.07			
03WN12	12.7–13.1	13.50	8.75		9.24	10.52					
03WN13	11.7–12.1	12.46	8.64		6.73	6.87					
03WN14	11.1–11.5	11.94	8.83		5.68	6.43					
Xiuning											
03WN33	12.4–12.8	13.24	9.83	10.14	10.34	10.03	6.10	9.08	6.06		6.71
03WN34	12.3–12.7	13.10	9.53	10.13	10.39	11.58	5.96	9.19			6.45
03WN35	12.6–13.0	13.37	9.53	9.87	10.54	10.38	6.31			10.67	
03WN55A	12.2–12.6	13.03	9.52	10.14	9.77	9.07	5.70			10.29	5.50
03WN55B	12.8–13.2	13.55	9.73	9.97	9.90	9.71	4.26	8.37			4.22
03WN56	12.1–12.5	12.88	9.78	10.16	9.83	10.12					5.20
03WN57	12.8–13.2	13.61	9.94		10.75	9.92	5.42				
03HN49	12.9–13.3	13.72	10.13		10.56	9.50	5.06				5.65
03HN50	13.2–13.6	14.02	9.97		10.92	9.80					
03HN51	12.5–12.9	13.30	10.23		10.72	9.05					

WR: estimate value of whole rock for primary magma; Qz: quartz; Zr: zircon; Gt: garnet; Pl: plagioclase; Kfs: potassic feldspar; Bi: biotite; Cor: cordierite; Ilm: ilmenite; Mus: muscovite; Chl: chlorite.

with breakdown of Al-rich micas (Patino Douce and McCarthy, 1998). The arc-like features of elements and isotopes suggest a marine environment for sedimentation of source rocks. However, the much more significant enrichment of LREE and LILE occurs in the granodiorites than in the arc basalts despite the similarity in Nb and Ta depletion pattern between them (Fig. 6b). If the arc basalts are assumed to be primitive protolith of the granodiorites, multistage melting and differentiation are required for the LREE and LILE enrichment.

On the other hand, their protolith has the geochemical nature of juvenile crust as indicated by the positive $\varepsilon_{Hf}(t)$ values of 3.8–4.4 for zircon (Fig. 11), the neutral $\varepsilon_{Nd}(t)$ values of −2.06 to 0.02 and the low to medium initial $^{87}Sr/^{86}Sr$ ratios of 0.7033–0.7087 for whole-rock (Table 7). The two highest $(^{176}Hf/^{177}Hf)_i$ ratios of 0.282523–0.282539 occur in inherited grains with U–Pb ages of 882 ± 16 Ma (Fig. 10), corresponding to the maximum $\varepsilon_{Hf}(t)$ values of 9.3–9.9 and the youngest T_{DM} ages of 989–1013 Ma (Table 4). The youngest T_{DM} ages are only about 100 Ma older than the crystallization ages of 882 ± 16 Ma for the inherited zircon, indicating its derivation from juvenile crust that evolved from depleted mantle due to crust–mantle interaction by island-arc magmatism before about 900 ± 20 Ma (Fig. 18). In fact, the averaged Hf model ages of 1.17 ± 0.08 to

Table 6
Oxygen isotopic temperatures for quartz-mineral pairs from Neoproterozoic granodiorite in South Anhui (in °C)

Sample	Qz–Zr	Qz–Gt	Qz–Pl	Qz–Kfs	Qz–Bi	Qz–Cor	Qz–Ilm	Qz–Mus	Qz–Chl
Xucun									
03WN15	540	720	115		265				240
03WN16	575	765	200	190	275				
03WN17	700		155						
03WN18	600	835	195		275	325			
03WN19	575	705			240				255
03WN27	600	810			230				
03WN28	635	790			220				
03WN29	630	865	230		280				
03WN30	615		235	105	290				
03WN31		780			315				275
03WN32	785		200	245	240				180
Shexian									
03WN01								400	
03WN02			190					430	
03WN03			215						
03WN04	615		130						
03WN05	565							415	
03WN06	550	595			265	105			
03WN09	580		235	155					180
03WN10	525		180						190
03WN11	610		275	135	330	280			
03WN12	515		180	230					
03WN13	630								
03WN14	740								
Xiuning									
03WN33	690	750	320	205	305	370	605		275
03WN34	615	775	345	520	305	395			270
03WN35	625	680	327	230	310			575	
03WN55A	615	790	270	140	295			565	225
03WN55B	630	670	230	150	210	280			155
03WN56	740	825	300	260	115				215
03WN57	650		325	160	255				
03HN49	660		285	120	235				200
03HN50	600		290	120	95				
03HN51	750		365	120					

Note: temperature calculation is based on the calibrations of Zheng (1991, 1993a, 1993b).

1.25 ± 0.06 Ga for the zircons (Fig. 12) with the positive $\varepsilon_{Hf}(t)$ values of 3.4 ± 1.6 to 5.4 ± 2.6 (Fig. 11) suggest the presence of a depleted mantle component in the magma sources of either the ca. 882 ± 16 Ma protolith or the 824 ± 6 Ma granodiorites.

As illustrated in Fig. 19, the zircon $\varepsilon_{Hf}(t)$ values positively deviate from the whole-rock $\varepsilon_{Nd}(t)$ values with reference to the normal terrestrial arrays of mantle and crust Hf–Nd isotope evolution (Vervoort et al., 1999), suggesting Hf–Nd isotope decoupling in the granodiorites. Abnormal enrichment of radiogenic Hf isotopes in terrestrial rocks is basically related to anomalously high Lu/Hf ratios in their source. Three possible mechanisms have been suggested to explain the whole-rock Hf–Nd isotope decoupling: (1) melt-peridotite interaction in the magma source of mantle-derived rocks. This has been suggested for the Hf–Nd isotope decoupling in the oceanic lithosphere (Bizimis et al., 2003), which is ascribed to metasomatism of either an ancient (e.g., 1 Ga or older) depleted peridotite protolith or 80–100 Ma depleted oceanic lithosphere by melting products of extensive mantle-melt interaction; (2) coexistence of garnet during zircon crystallization from magma. As suggested by Vervoort et al. (2000), the Hf–Nd isotope decoupling can result either from melt extraction in the presence of garnet to produce higher Lu/Hf ratios in a restite, or from crystallization of garnet from a magma to bring about high Lu/Hf ratios in a cumulate. Both processes involve the role of garnet because this mineral is significantly enriched in HREE, resulting in the

Table 7
Summary of zircon U–Pb age and Lu–Hf isotopes, whole-rock Sm–Nd and Rb–Sr isotopes, and mineral O istopes for Neoproterozoic granodiorites in South Anhui

Sample number	U–Pb age		Lu–Hf isotope		Sm–Nd isotope			Rb–Sr isotope	$\delta^{18}O$ (‰)	
	t_2 (Ma)	t_1 (Ma)	$\varepsilon_{Hf}(t)$	T_{DM} (Ga)	$\varepsilon_{Nd}(t)$	T_{DM1} (Ga)	T_{DM2} (Ga)	I_{Sr} (t)	Quartz	Zircon
Xucun										
03WN15					0.02	1.59	1.49	0.706107	13.94	9.38
03WN19	827 ± 7	871 ± 6			−0.52	1.62	1.53	0.705090	13.48	9.25
03WN29	823 ± 7	878 ± 14	5.4 ± 2.69	1.17 ± 0.8	−0.45	1.60	1.52	0.707362	13.28	9.47
03WN31					−1.14	1.70	1.58	0.704390	13.09	
Shexian										
03WN01					−2.06	1.74	1.65	0.708583	13.09	
03WN05	823 ± 9	882 ± 8	3.4 ± 1.6	1.25 ± 0.06	−1.33	1.65	1.60	0.708700	13.85	
03WN10	824 ± 6	891 ± 21			−1.71	1.75	1.63	0.707347	13.91	
03WN13					−0.43	1.59	1.52	0.708015	12.46	
Xiuning										
03WN33					−0.73	1.71	1.55	0.703389	13.24	9.83
03WN35					−0.70	1.68	1.54	0.706458	13.37	9.53
03HN49	824 ± 7	892 ± 14	3.5 ± 0.9	1.24 ± 0.04	−0.60	1.65	1.54	0.705431	13.72	10.13
03HN51	825 ± 7	913 ± 11			−1.00	1.72	1.57	0.704480	13.30	10.23

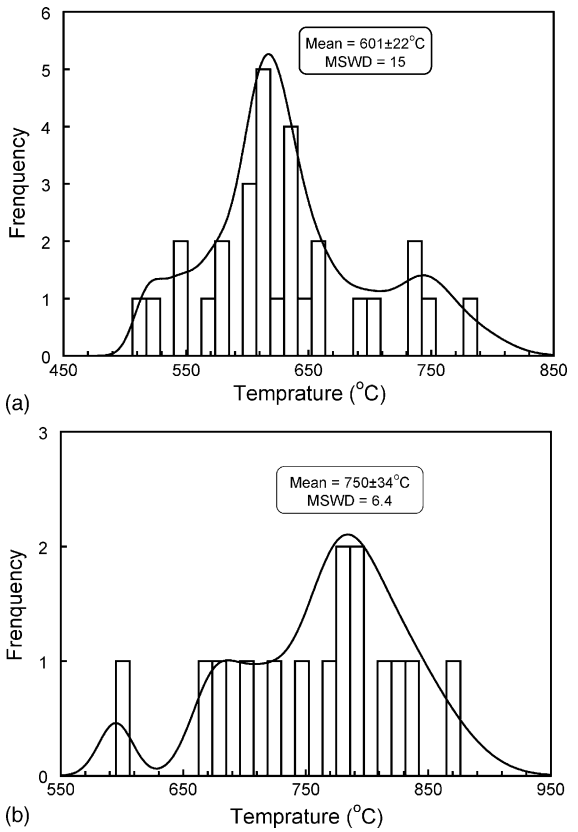

Fig. 16. Histogram of O isotopic temperatures between quartz and other minerals from Neoproterozoic granodiorites in South Anhui: (a) quartz–zircon pairs and (b) quartz-garnet pairs.

preferential incorporation of Lu over Hf; (3) seawater involvement prior to partial melting of source rocks. It is known that for a given $\varepsilon_{Nd}(t)$ value the corresponding $\varepsilon_{Hf}(t)$ value is higher for seawater than it is for the terrestrial (mantle–crust) rocks (e.g., Alberade et al., 1998; Piotrowski et al., 2000; van de Flierdt et al., 2002). The melt-peridotite interaction is not necessary for generation of arc-derived igneous rocks and their anatectic product granodirites, so that the Hf–Nd isotope decoupling cannot be ascribed to this mechanism. Depletion of

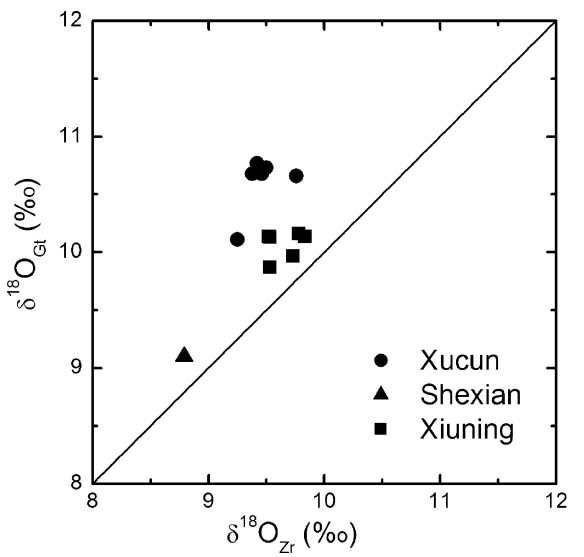

Fig. 17. Plot of garnet $\delta^{18}O$ vs. zircon $\delta^{18}O$ values for Neoproterozoic granodiorites in South Anhui.

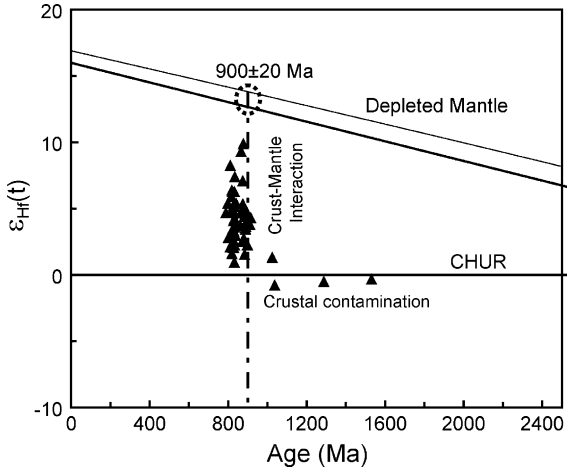

Fig. 18. Schematic diagram for Lu–Hf isotopic evolution vs. U–Pb age for zircons from granodiorites at the southeastern margin of the Yangtze Block. The thin line denotes the evolution of depleted mantle (DM) with a present-day $^{176}Hf/^{177}Hf = 0.28325$ and $^{176}Lu/^{177}Hf = 0.0384$ (Griffin et al., 2000), and the thick line denotes the evolution of depleted mantle that is drawn by using $\varepsilon_{Hf}(t) = 16$ at $t = 0$ Ma for MORB at present (average MORB value, Nowell et al., 1998) and $\varepsilon_{Hf}(t) = 6$ at $t = 2.7$ Ga (Corfu and Noble, 1992; Vervoort et al., 1999). Crust–mantle interaction is supposed to occur during arc magmatism before arc-continent collision at about 900 ± 20 Ma, but its record of zircon Lu–Hf and U–Pb isotopes becomes effective by reworking of arc crust during syn-collisional magmatism. Both source mixing and crustal contamination were involved during magmatism of granodiorite protolith, with variable degrees of incorporation of crustal components.

HREE relative to LREE is indeed observed for the granodiorites in South Anhui (Fig. 6a). This is consistent with the presence of residual garnet in their source, but the HREE depletion relative to LREE in crustal rocks can also be produced by geochemical differentiation during partial melting. Furthermore, the REE pattern in Fig. 6b is not typical for residual garnet in the source because a progressive decrease in HREE is commonly expected with atomic number when garnet is crystallizing. Thus the second mechanism is less possible. The high A/CNK ratios and $\delta^{18}O$ values were obtained for the granodiorites (Tables 2 and 6), indicating that the chemical weathering and sedimentation of juvenile crust occurred in the marine environment. Although the seawater was inevitably involved in the sedimentary source of S-type granites, the difference in the Hf isotope composition between seawater and the dissolved bulk continental crust is generally considered to be due to retention of unradiogenic Hf in resistant zircons during incomplete weathering of continental crust (van de Flierdt et al., 2002). The most likely cause of the higher $^{176}Hf/^{177}Hf$ ratio of seawater at a given $^{143}Nd/^{144}Nd$ ratio is that the normal erosion of continents involves incongruent weathering (Piotrowski et al., 2000). That is, the Hf isotope composition of river waters should be more radiogenic relative to the bulk composition of their source rocks. However, the chemical weathering and sedimentation of arc-derived rocks normally occur in such marine environments as fore-arc and back-arc basins, with much more involvement of seawater than river waters. Thus the third mechanism is also less possible for the mismatch in the Hf–Nd isotope composition between the Anhui granodiorites and the normal terrestrial rocks.

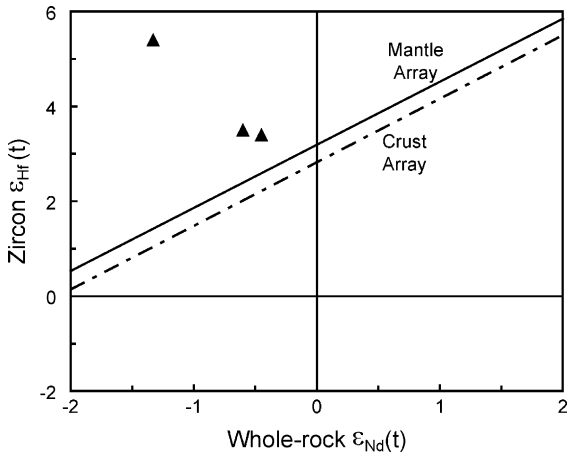

Fig. 19. Relationship between zircon $\varepsilon_{Hf}(t)$ and whole-rock $\varepsilon_{Nd}(t)$ values at $t = 824$ Ma for Neoproterozoic granodiorites in South Anhui. Mantle and crust arrays are from to Vervoort et al. (1999).

Because zircon is a resistant and refractory mineral during chemical weathering and partial melting, it is capable of preserving its primary Hf isotope composition of magma crystallization. Thus we explain the decoupling of zircon Hf versus whole-rock Nd isotopes in the Anhui granodiorites as being due to retention of radiogenic Hf in igneous zircons during chemical weathering and partial melting of arc-derived crust. It is suggested that zircon retains its Hf isotope signature acquired during crystallization from arc-derived magma, whereas the whole-rock Sm–Nd system was readily equilibrated with the new melt and hence gave the lower $\varepsilon_{Nd}(t)$ values. As a result, the granodiorites have the less radiogenic Nd isotope compositions than the normal terrestrial rocks, and the zircons that crystallized from such an evolved source show the high $\varepsilon_{Hf}(t)$ ratios above the Hf–Nd terrestrial array (Fig. 19). This may also explain the observation from the granodiorites in South Anhui that the zircon Hf model ages (Table 4) are significantly younger than the whole-rock Nd model ages (Table 3). It appears that zircon Lu–Hf and whole-rock Sm–Nd isotope systems in arc-derived rocks were evolved in different ways, with significant difference in their element concentrations and isotope compositions.

Furthermore, the protolith of the granodiorites would be derived from a relatively more depleted mantle source than its anatectic product that incorporated more components of evolved crust during magmatism at ca. 820 Ma. The core and rim of one zircon grain with different $^{206}Pb/^{238}U$ ages of 820 ± 10 and 868 ± 11 Ma also has different $\varepsilon_{Hf}(t)$ values of 1.6 and 4.7 (Fig. 13a), indicating that the young domain with the low $\varepsilon_{Hf}(t)$ value involves the incorporation of crustal component by fluid/melt infiltration during partial melting to result in anatectic recrystallization. In this regard, partial melting causes newly grown zircon to have a decreased $^{176}Hf/^{177}Hf$ ratio, contrasting with a metamorphic effect that results in newly grown zircon having an increased $^{176}Hf/^{177}Hf$ ratio (Zheng et al., 2005).

The Rb/Sr ratios of 0.48–0.96 for the granodiorites in South Anhui are less than 3, suggesting that they were generated by fluid-present melting of a psammitic source (Harris and Inger, 1992; Sylvester, 1998). This is consistent with the Shangxi Group metasediments, which mainly consist of sandstone and arenaceous phyllite (Anhui, 1987). Retained phyllite enclaves and crustal enclaves such as cordierite-bearing mica schist and andalusite schist were identified (Xing et al., 1988; Shen et al., 1999). Thus it is inferred that the granodioritic magmas may form in a collision-thickened orogen, derived from melting of sedimentary rocks like the Shangxi Group. A similar situation also occurred in the late-Paleozoic peraluminous granites of the eastern Urals, where Gerdes et al. (2002) interpreted them to be related to relatively rapid rebuilding of juvenile arc crust and deep burial of the source rocks.

On the basis of our zircon U–Pb dates, most of the inherited zircons from the granodiorites in South Anhui have $^{206}Pb/^{238}U$ ages of 871 ± 6 to 913 ± 11 Ma (Table 7), with a cluster at 882 ± 16 Ma (Fig. 4b). From the CL images (Fig. 2) it can be seen that many of the inherited zircons are long prismatic (about 100–200 μm in length), with variable length/width ratios of about 1–6. Although the great length/width ratio is more diagnostic of volcanic zircon than plutonic zircon, both types of zircon may occur in the source. This suggests the presence of ~880 Ma magmatism at the southeastern margin of the Yangtze Block. The REE and trace element features of the granodiorites in South Anhui are similar to those of arc basalts (Fig. 6), and thus may be inherited from similar source rocks. Therefore, it is inferred that extensive magmatism took place at ca. 900 ± 20 Ma due to arc-continent collision between the Cathaysia and Yangtze Blocks.

The 882 ± 16 Ma arc-derived igneous rocks in South Anhui may possibly have formed in a suprasubduction zone (SSZ) setting. In such a tectonic setting, the time interval between syn-collisional magmatism and deposition of its weathered clastics is very short, generally less than several million years (Hawkins, 2003), so that they are considered to be quasi-coeval. The arc-derived intrusives in the suprasubduction zone can be rapidly weathered and deposited in fore-arc and back-arc basins to form huge thicknesses of juvenile clastic sediments. In fact, the Shangxi Group metasediments range up to ~13.3 km in thickness (Anhui, 1987). Single-stage Nd model ages of 1.63–1.69 Ga for the Shangxi Group metasedimentary rocks (Cheng, 1993) are similar to the T_{DM1} ages of 1.59–1.75 Ga for the granodiorites in South Anhui (Table 7). In addition, the zircon $\varepsilon_{Hf}(t)$ values of 3.4–5.4 and T_{DM} ages of 1.17–1.25 Ga for the granodiorites (Figs. 11 and 12) are comparable with whole-rock $\varepsilon_{Nd}(t)$ values of 3.0–6.2 and the T_{DM1} ages of 1.28–1.16 Ga for the ca. 910–870 Ma magmatic rocks in North Zhejiang (Shen et al., 1999). These facts suggest that syn-collisional magmatism at ca. 900 ± 20 Ma involved reworking of pre-existing arc crust that bears a major contribution from a depleted mantle source.

On the other hand, the oldest $^{206}Pb/^{238}U$ ages of 1024–2444 Ma are associated with the lowest $(^{176}Hf/^{177}Hf)_i$ ratios of 0.281459–0.282250 with negative $\varepsilon_{Hf}(t)$ values of −28.4 to −0.3 and high Hf model ages of 1400–2466 Ma (Table 4). This clearly indicates that old crustal relicts of Paleoproterozoic to Mesoproterozoic age were added to the sediments of juvenile crust during either the protolith magmatism at 882 ± 16 Ma or the granodioritic magmatism at 824 ± 6 Ma. This is consistent with a setting of arc-continent collision along the southeastern margin of the Yangtze Block during the early Neoproterozoic.

When the S-type granodiorites in South Anhui were formed at ca. 824 ± 6 Ma (Fig. 4a), the arc-continent collision setting had been transformed into an extensional accretionary orogen (see Collins, 2002). The deposition of weathered juvenile crust occurred in the period from about 880 to 830 Ma, synchronous with such transformation in such a tectonic setting. The time interval between the syn-collisional magmatism (882 ± 16 Ma) and magma emplacement (824 ± 6 Ma) from anatexis of arc-derived clastic sediments is ca. 40–80 Ma. A similar situation also occurred in the Lachlan Fold Belt of southeastern Australia, where S-type granites intruded at ca. 420–430 Ma containing inherited zircons with U–Pb ages of 443–495 Ma (Keay et al., 1999). This suggests that weathered sediments from Ordovician magmatic rocks were remelted during the early Silurian, with a time interval of ca. 20–70 Ma between magmatism of their source rocks and S-type granite emplacement. Stud-

ies of Archean and Paleoproterozoic magmatic rocks also show that time intervals between volcanic eruption of mantle-derived magma and intrusion of syntectonic granite are about 50–80 Ma (Kemp and Hawkesworth, 2003). Because the emplacement of post-collisional S-type granodiorite in South Anhui is only 40–80 Ma later than the arc-continent collision, the granodiorites remelted from the young sediments of juvenile crust have the unusual petrological, element and isotope geochemical features of both S- and I-type granites.

5.2. Petrogenetic temperatures and alteration

Previous petrological studies reported quite scattered temperatures for the granodiorites in South Anhui. Zhou and Wang (1988) obtained temperatures of 780–820 °C based on phase equilibrium between cordierite, almandine, biotite, plagioclase and quartz following the experiments of Green and Usdansky (1986). Together with the mineralogical features of Al-rich minerals and feldspars from the intrusives, the authors interpreted the granodiorites to be emplaced at medium to deep crustal levels (depths of 8–24 km). By contrast, in terms of the chemical compositions of whole-rock and biotite, Xing et al. (1988) calculated a temperature of ca. 700 °C and a depth of 9.3 km for crystallization of the Shexian granodiorite. According to the Zr contents and whole-rock major element composition, Zr saturation temperatures of 829 ± 18 °C were acquired in this study (Table 2 and Fig. 7). Because zircon is one of the first minerals to crystallize from magma, the Zr saturation temperatures are close to the liquidus temperature (e.g., Ferreira et al., 2003). Thus we interpret 829 ± 18 °C as the initial temperature of magma crystallization for the granodiorites in South Anhui. Nevertheless, the low Al_2O_3/TiO_2 ratios of 23.4–50.8 for these rocks suggest that melting temperatures would be higher, probably above ~875 °C (Sylvester, 1998). The temperature seems rather high for S-type granites and more of what are expected for A-types. The reason for such high temperatures may lie in the fact that this is a special category of S-type granites that was derived from reworking of juvenile crust. The O isotope temperatures are 750 ± 34 °C for the quartz-garnet pairs (Table 6 and Fig. 16b), apparently representing the closure temperature of O diffusion in garnet during magma crystallization and cooling.

According to the calibrations of Zheng (1993a, 1999) and Valley (2003), the differences in $\delta^{18}O$ value between zircon and garnet at O isotope equilibrium are about 0.1 ± 0.2‰. Thus the two minerals would have identical O isotope temperatures if they could have the same rates of O diffusion during magma cooling. The mean O isotope temperature of 601 ± 22 °C for the quartz–zircon pairs is significantly lower than that of 750 ± 34 °C for the quartz-garnet pairs (Table 6 and Fig. 16a and b), and the $\delta^{18}O$ values of zircon are considerably lower than those of garnet (Fig. 17). These suggest that the coexisting zircon and garnet were in isotopic disequilibrium with each other. This can be caused by either difference in O transport rate between the two minerals or inheritance of O isotopes in zircon. Because of the very slow rate of O diffusion in crystalline zircon (Watson and Cherniak, 1997; Zheng and Fu, 1998), the zircon is capable of preserving its magmatic $\delta^{18}O$ value through subsequent dry granulite-facies metamorphism, subsolidus hydrothermal alteration, and possibly magmatic assimilation or anatexis (Valley, 2003; Zheng et al., 2004).

The samples from the Xucun pluton contain more inherited zircons than those from the Xiuning pluton (Fig. 2), which may have evolved from mantle-derived magmas with relatively low $\delta^{18}O$ values. As a result, the $\delta^{18}O$ differences of 0.9–1.4‰ between garnet and zircon are also greater than those of 0.2–0.6‰ for the Xiuning pluton (Fig. 17). In this regard, the lower O isotope temperature of 601 ± 22 °C for the quartz–zircon pairs is possibly caused by the presence of a considerable proportion of inherited zircons with relatively lower $\delta^{18}O$ values that may be close to 5.3 ± 0.3‰, typical of normal mantle zircons. According to the measured $\delta^{18}O$ values for quartz, $\delta^{18}O$ values of 8.8–11.0‰ can be calculated for coexisting zircons at 750 °C. If 75–90% of magmatic zircons (with $\delta^{18}O$ values of 8.8–11.0‰) are mixed with 10–25% of inherited zircons (with $\delta^{18}O$ value of 5.3‰), then $\delta^{18}O$ values of the mixture are 8.0–10.4‰ that agree well with the measured $\delta^{18}O$ values of 8.0–10.3‰ for the zircons. As a result, the measured $\delta^{18}O$ values for the zircons are lower than those for the garnets (Table 5), and the inherited zircons have partially preserved their protolith $\delta^{18}O$ values when the arc-derived rocks were partially molten to generate the granodioritic magma. In this regard, the elevated $\delta^{18}O$ values for igneous zircon can only result from anatexis of the high $\delta^{18}O$ S-type granite source that underwent low-T water–rock interaction prior to the melting.

All the granodiorites from South Anhui have high LOI contents of 1.6–4.1% with a predominant part of water (Table 2), indicating that they underwent different degrees of post-magmatic alteration. Significant alteration is also evident from the zircon CL images (Fig. 2); nevertheless, the euhedral shape, with oscillatory zoning, has been well preserved. Because the relatively refractory minerals such as zircon and garnet have slow rates of O diffusion (Watson and Cherniak, 1997; Zheng and Fu,

1998) and thus high closure temperatures of O isotope exchange during cooling, they are capable of preserving their original $\delta^{18}O$ values during subsolidus hydrothermal alteration (Zheng et al., 2004). Thus the high $\delta^{18}O$ values for the refractory minerals from the granodiorites (Table 5) suggest the occurrence of secondary magmas with high $\delta^{18}O$ values. This is in stark contrast with low and negative $\delta^{18}O$ values for the bimodal igneous rocks of middle Neoproterozoic age that occur along the northern margin of the Yangtze Block (Zheng et al., 2004), where both supersolidus water–rock interaction and low-^{18}O magmatism have been suggested along rifting tectonic zones for their petrogenesis. For the granodiorites in South Anhui, however, the hydrothermal alteration during magma emplacement and cooling took place at subsolidus temperatures. No conspicuous infiltration of low $\delta^{18}O$ surface water and high-T hydrothermal alteration at supersolidus conditions can be identified from its effect on refractory mineral O isotope composition. This indicates that the granodiorites were formed in a pre-rift phase, with the elevated $\delta^{18}O$ values for the rock-forming minerals owing to the chemical weathering of source rocks. A syn-rift phase can be excluded since it is characterized by the occurrence of lower $\delta^{18}O$ values than the normal mantle $\delta^{18}O$ values $5.7 \pm 0.3‰$ for rock-forming minerals due to supersolidus water–rock interaction (and even low-^{18}O magmatism).

On the other hand, non-refractory minerals such as K-feldspar, plagioclase, biotite and cordierite from the granodiorites show large $\delta^{18}O$ variations with somewhat decreased $\delta^{18}O$ values, indicating that they were subject to different degrees of hydrothermal alteration at subsolidus temperatures. This results in the decrease in $\delta^{18}O$ values for the non-refractory minerals and the destruction of O isotope equilibrium fractionations between the refractory and non-refractory minerals. Non-uniform alteration appears to occur in the rocks at the post-magmatic stage, in association with short-lived kinetic effects on O isotope exchange between the minerals of different O diffusion rates during water–rock interaction (Criss et al., 1987; Gregory et al., 1988). According to the measured quartz $\delta^{18}O$ values, the calculated $\delta^{18}O$ values for coexisting K-feldspar, plagioclase, biotite and cordierite in equilibrium with quartz at 800 °C are 10.9–13.1‰, 10.7–12.9‰, 9.1–11.3‰ and 9.9–12.1‰, respectively. However, the actual measured $\delta^{18}O$ values are 4.5–11.6‰, 5.6–10.9‰, 4.2–6.5‰ and 4.2–9.2‰, respectively (Table 5). Clearly, the $\delta^{18}O$ values of hydrothermal fluid are significantly lower than the typical mantle whole-rock $\delta^{18}O$ values of $5.7 \pm 0.5‰$ (Harmon and Hoefs, 1995). They may be close to about 0‰ like seawater, with a possible origin from interstitial water within marine sedimentary rocks. The seawater-like fluid should come from the metasedimentary rocks themselves, since they melted to give rise to the granodiorites and the subsequent alteration was subsolidus. Thus, this is a kind of deuteric fluids that are cognate and evolved from within the system. Nevertheless, it remains to resolve whether or not such low $\delta^{18}O$ fluids were derived from exsolution of structural hydroxyl dissolved in igneous minerals. Meteoric water in a cold paleoclimate can be excluded because it may have $\delta^{18}O$ values of −16 to −10‰ (Zheng et al., 2003a).

Commonly, the O isotope exchange continued under subsolidus conditions after magma crystallization. Such isotope exchange is principally controlled by the rates of O diffusion in minerals during cooling and is thus a function of both cooling rate of the granite and fluid availability for infiltration. Discordant O isotope temperatures for the different quartz-mineral pairs usually suggest reequilibrated fractionations between quartz and the minerals with different rates of O diffusion (Giletti, 1986; Eiler et al., 1993). Nevertheless, the observed sequence of mineral-pair O isotope temperatures for the granodiorites in South Anhui is concordant with the closure temperatures estimated from the rates of O diffusion in these minerals (Zheng and Fu, 1998; Zhao et al., 2004), suggesting the presence of retrograde isotope exchange during granite cooling.

The closure temperature of element diffusion is normally defined for one mineral by assuming that it depends on diffusion in one mineral under close-system conditions (Dodson, 1979). When applying the O isotope geothermometry to intrusive rocks, however, it has been a common practice to pair quartz with other minerals. Substantially, quartz and the every other mineral do not have the same rate of O diffusion and thus the same closure temperature. Therefore, a potential assumption in the quartz–mineral geothermometers is that quartz behaves isotopically as an infinite reservoir for O isotope exchange with every other mineral during cooling. Although the assumption has not been proven so far, its validity is favored by the following consensus: (1) the common success in applying the O isotope geothermometers to igneous and metamorphic rocks in nature; (2) the common occurrence of two SiO_2 polymorphs as α- and β-quartz in the high-temperature rocks, which show negligible O isotope fractionations between them (Zheng, 1993a); (3) the substantial presence of SiO_2 composition in silicate rocks. In this regard, SiO_2 may behave isotopically as a pervasively active phase for O diffusion within natural silicate rocks in high-temperature geological processes (Zheng et al., 2003b).

5.3. Reworking of juvenile crust

The Sm–Nd isotope data of Zhou et al. (1989) and Chen et al. (1991) for the Fuchuan ophiolites in South Anhui were recalculated by Li et al. (1997) who gave much large errors for two isochron ages of 1010 ± 89 and 934 ± 84 Ma. SHRIMP zircon U-Pb dating for adakitic granite within the ophiolite in Northeast Jiangxi yielded an age of 968 ± 23 Ma (Li et al., 1994), which is re-interpreted as the timing of subduction of oceanic crust (Li and Li, 2003). TIMS zircon U–Pb ages for volcanics from the Xiaojiwa–Hanyangfeng Formation in North Jiangxi are 917 ± 36 and 878 ± 51 Ma, respectively (Xie et al., 1997). There are a lot of arc-like igneous rocks with zircon U–Pb ages of ca. 900 ± 20 Ma in North Zhejiang (Cheng, 1993; Shen et al., 1999). This study indicates the cryptic occurrence of 882 ± 16 Ma igneous rocks along the Jiangnan Fold Belt. Because the age of 882 ± 16 Ma is responsible for the predominant population of inherited zircons in the granodiorites in South Anhui (Figs. 2, 3 and 4b), it appears that juvenile crust of this age with geochemical similarities to the exposed arc-derived rocks between the Yangtze and Cathaysia Blocks not only underlies much of the Jiangnan Fold Belt but also forms a major component in the granodiorite sources. Arc magmatism probably took place from about 1.1 to 0.9 Ga in the southeastern margin of the Yangtze Block, corresponding to Grenville-age subduction of oceanic crust with progressive convergence between the Yangtze and Cathaysia Blocks. The arc-continent collision is thus suggested to occur at about 900 ± 20 Ma, resulting in reworking of arc crust by syn-collisional magmatism with the incorporation of crustal materials as suggested by the zircon Lu–Hf isotope evolution (Fig. 18).

Besides the present LA-ICPMS U–Pb dates at 824 ± 6 Ma for the granodiorites in South Anhui (Fig. 4a), a number of SHRIMP zircon U–Pb dates are also available for Neoproterozoic igneous rocks along the southeastern margin of the Yangtze Block. The Bendong granodiorite and the Sanfang granite in North Guangxi have $^{206}Pb/^{238}U$ ages of 818 ± 10 and 827 ± 15 Ma, respectively (Li, 1999). Andesitic agglomerate of volcaniclastic rocks in the lower part of the Cangshuipu Formation in Hunan Province has a $^{206}Pb/^{238}U$ age of 814 ± 12 Ma (Wang et al., 2003a). The Jiuling granite in North Jiangxi has a $^{206}Pb/^{238}U$ age of 819 ± 9 Ma (Li et al., 2003a). Rhyolite from the Taoyuan Formation in Northeast Jiangxi has a $^{206}Pb/^{238}U$ age of 818 ± 12 Ma (Wang et al., 2003b). Even bimodal magmatism at 818 ± 9 Ma is found in the northwestern margin of the Cathaysia Block (Li et al., 2005). Extensive magmatic activity at ca. 830–740 Ma in South China has been hypothesized as being related to the Rodinia breakup, triggered by a mantle superplume (Li et al., 1995, 1999, 2003a, 2003b). Since the partition patterns of trace elements in some of these rocks are similar to those typical of island-arc volcanics, an island-arc origin is suggested for their petrogenesis (Wang et al., 2004a, 2004b; Zhou et al., 2004). While the former hypothesis ascribes the magmatism to the supercontinent breakup, the latter suggestion associates their generation with subduction of oceanic crust during supercontinent assembly.

If a superplume event is defined as a short-lived mantle event lasting ≤100 Ma (Condie, 2001), this superplume consisting of many small plumes rise through the mantle in this period and bombards the base of the continental lithosphere. As a result, such large igneous provinces as komatiites, flood basalts, mafic dyke swarms, and layered mafic intrusions form as a type of surface exposures (Ernst and Buchan, 2003). In this regard, a critical question regarding a proposed plume at any locality is where is the mantle plume? So far no actual material specifically related to a mantle plume has been identified in any of the 830–820 Ma igneous rocks along the Jiangnan Fold Belt between the Cathaysia and Yangtze Blocks. No the large igneous provinces of any type in this age has been found in South China either. Thus this episode of Neoproterozoic magmatism is difficultly interpreted as the product of mantle superplume activity.

Although supercontinent breakup may be triggered by the impingement of a superplume on the overlying lithosphere (Morgan, 1981; Richards et al., 1989; Hill, 1991; Storey and Kyle, 1997; White, 1997), it can also be caused by lithospheric extension in response to subduction (Anderson, 1982; Le Pichon and Huchon, 1984; Cox, 1988; Storey et al., 1992). Because ancient collisional belts are favorite places for rift magmatism and continental breakup (Dewey, 1988; Vauchez et al., 1997; Tommasi and Vauchez, 2001), attributes of orogenic lithosphere are susceptible to reactivation by extensional tectonics and thermal anomalies. Because the Yangtze and Cathaysia Blocks did not split up along the Jiangnan Fold Belt during the initial separation of South China from Rodinia at ~750 Ma (Zheng et al., 2006), extensional collapse of the arc-continent collision orogen is suggested to cause the melting of evolved arc-derived sediments and underlying substrate at 830 to 820 Ma. Thickened lithospheric mélange of the suture zone would easily undergo partial melting to produce melts with a similar crustal heritage. As a result, the extensional collapse of the collision-thickened orogen along the southeastern margin of the Yangtze Block

gives rise to the S-type magmatism at 824 ± 6 Ma, with major derivation from melting of arc-like orogenic sediments. Therefore, the reworking of juvenile arc crust by syn-collisional magmatism at about 882 ± 16 Ma has provided the source for the 824 ± 6 Ma granodiorites in South Anhui.

In addition, melting of an orogenic lithospheric keel is favored by an additional heat supply from asthenospheric upwelling in extensionally collapsed orogens (Thompson and Connolly, 1995). If a mantle superpwelling did exist at ca. 825 Ma elsewhere in the world as a dynamic response to lithospheric extension, a coeval mantle upwelling could be supposed to occur at the southeastern margin of the Yangtze Block that might facilitate the melting of orogenic lithospheric keel. Nevertheless, extensive magmatism of island-arc and back-arc types would have taken place during the subduction of oceanic crust and subsequent convergence between the two continents at about 1.1–0.88 Ga, respectively, resulting in igneous rocks of arc-like and rift-like geochemistry. In this regard, the closure of back-arc basins by arc-continent collision would produce the source rocks of S-type granitoids between the Yangtze and Cathaysia Blocks. While the island-arc magmatism has transferred the depleted mantle material to arc crust, the arc-continent collision and its associated magmatism may serve as a basic mechanism to change the bulk composition of arc crust to be more continental (Rudnick,

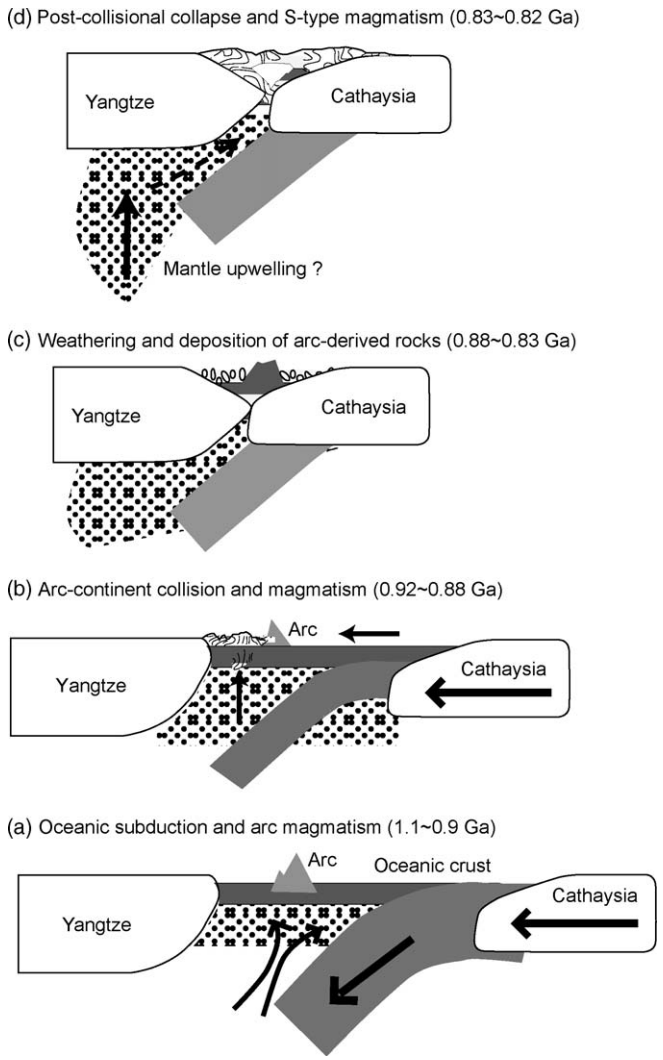

Fig. 20. Sketch model for Neoproterozoic tectonic evolution between the Yangtze and Cathaysia Blocks with respect to (a) subduction of oceanic crust and island-arc magmatism between 1100 and 900 Ma, (b) arc-continent collision and syn-collisional magmatism at 900 ± 20 Ma, (c) chemical weathering and marine deposition of arc-derived igneous rocks between 880 and 830 Ma, and (d) post-collisional collapse and S-type magmatism at 830–820 Ma to generate the granodiorites in South Anhui.

1995; Holbrook et al., 1999; Draut et al., 2002). This points to a significant contribution by the reworking of arc crust to continental growth.

On the basis of the above discussion, the origin of granodiorites in South Anhui can be summarized as follows: (1) Grenvillian oceanic crust was progressively subducted at ca. 1.1–0.9 Ga between the Yangtze and Cathaysia Blocks (Fig. 20a), with arc magmatism close to the continental margin of the Yangtze Block; (2) arc-continent collision and magmatism occurred at about 900 ± 20 Ma at the southeastern margin of the Yangtze Block (Fig. 20b), with progressive emplacement of arc-derived magma and ophiolites in the suprasubduction zone; (3) the arc-derived igneous rocks underwent rapid weathering and deposition shortly after syn-collisional magmatism, resulting in low-maturity sedimentary rocks with high A/CNK ratios, high $\delta^{18}O$ values, neutral $\varepsilon_{Nd}(t)$ values and low initial $^{87}Sr/^{86}Sr$ ratios. The sediments derived from juvenile crust formed in the period from about 880 to 830 Ma (Fig. 20c); (4) due to extensional collapse of the collision-thickened orogen with a potential overprint by a thermal pulse (mantle upwelling?) at about 830–820 Ma that heated the orogenic root, the S-type granodiorites were generated by burial and melting of water-rich sedimentary rocks in the orogen (Fig. 20d). This episode of post-collisional magmatism occurs extensively at the periphery of the Yangtze Block, possibly marking not only the final assembly between the Yangtze and Cathaysia Blocks but also the onset of rift tectonics along the arc-continent collisional orogen. Although collapsed orogens are not a preferred site of continental rifting, a transformation of geotectonic framework from compressional to extensional regimes would take place at this time in South China. Splitting of South China from Rodinia appears to occur along its northern margin at about 750 Ma (Zheng et al., 2006).

6. Conclusions

Neoproterozoic granodiorites in South Anhui were generated at 824 ± 6 Ma, and their protolith formed at 882 ± 16 Ma with incorporation of some older Meso- and Paleoproterozoic components. In CL images, the young zircons are new grains or rims of homogeneous structure with magmatic zoning, whereas most of the old ages were obtained from cores or single xenocrysts. The granodiorites have high A/CNK ratios and high whole-rock $\delta^{18}O$ values, pointing to a supracrustal origin characteristic of S-type granites. They also have positive $\varepsilon_{Hf}(t)$ values for zircon, neutral $\varepsilon_{Nd}(t)$ values and low to medium initial $^{87}Sr/^{86}Sr$ ratios for whole-rock, indicating a magmatic source with significant components of juvenile crust, similar to I-type granites. Although there is no significant difference in $\varepsilon_{Hf}(t)$ between the two generations of zircon, some of the highest $\varepsilon_{Hf}(t)$ values are associated with the old zircons with $^{206}Pb/^{238}U$ ages of 882 ± 16 Ma. In addition, a few detrital zircons with Mesoproterozoic to Paleoproterozoic U–Pb ages have lower $\varepsilon_{Hf}(t)$ values and older Hf model ages than the Neoproterozoic zircons. These indicate that the granodioritic protolith was principally derived from a depleted mantle source, but that its anatectic product became relatively enriched with arc-like partition patterns for trace elements due to crust-mantle differentiation, with minor incorporation of ancient crustal components, during arc magmatism and subsequent reworking by chemical weathering and partial melting. Therefore, the granodiorites were produced by melting of the sediments of juvenile crust that was a primary contribution to the arc. They were then formed at about 824 ± 6 Ma by extensional collapse of the arc-continent collision orogen. As a result, the granodiorites are characterized by the features of both S- and I-type granites because of the short-term recycling of juvenile crust.

It appears that a cyclical process took place between the Cathaysia and Yangtze Blocks during the Early Neoproterozoic, including subduction of oceanic crust, island-arc magmatism, arc-continent collision and juvenile crust melting, uplift-erosion and sedimentation, post-collisional collapse and anatexis. This process not only mixed the newly derived mantle material with sedimentary component of the new crust, but also effectively differentiated the composition of juvenile crust. While growth of juvenile crust is assumed to occur by arc magmatism at 1.1–0.9 Ga, reworking of juvenile crust is concluded to take place by the two episodes of magmatism, respectively, due to arc-continent collision at about 900 ± 20 Ma and post-collisional collapse at 824 ± 6 Ma. It is the reworking of arc crust by syn- and post-collisional magmatism that drives bulk crust composition toward a more continental one. In this regard, arc-collision is not only a crucial step of the Wilson cycle by which intra-oceanic arc crust is added to continental margins, but also an important way by which the continental crust is built during the late Precambrian. Although intra-oceanic arc crust is too mafic to be a direct analogue for continental crust, the prominent enrichment of LREE and LILE in the granodiorites relative to the arc basalts provides compelling evidence to suggest a mechanism for compositional evolution from the arc crust to the continental crust by the multistage reworking via syn- and post-collisional magmatism in the arc-continent collision zone.

Acknowledgments

This study was supported by funds from the Natural Science Foundation of China (40334036) and Chinese Academy of Sciences (KZCX3-SW-141). Element and radiogenic isotope analyses were partly supported by the Laboratory of Isotope Geochronology and Geochemistry at the Guangzhou Institute of Geochemistry. We appreciate the assistance of H.L. Yuan with LA-ICPMS U–Pb dating, L.W. Xie and Y.Y. Yang with LA-MC-ICPMS Lu–Hf analysis, Z.Y. Chen with zircon CL imaging, D.E. Wang with field work, and B. Gong, X.P. Zha and Y.B. Zhao with O isotope analyses. Thanks are due to Dr. S. Wilde and an anonymous reviewer for their constructive comments that greatly help improvement of the manuscript.

References

Alberade, F., Simonetti, A., Vervoort, J.D., Blichert-Toft, J., Abouchami, W., 1998. A Hf–Nd isotope correlation in ferromanganese nodules. Geophys. Res. Lett. 25, 3895–3898.

Amelin, Y., Lee, D.C., Halliday, A.N., Pidgeon, R.T., 1999. Nature of the Earth's earliest crust from hafnium isotopes in single detrital zircons. Nature 399, 252–255.

Amelin, Y., Lee, D.C., Halliday, A.N., 2000. Early-middle Archean crustal evolution deduced from Lu–Hf and U–Pb isotopic studies of single zircon grains. Geochim. Cosmochim. Acta 64, 4205–4225.

Anderson, D., 1982. Hotspots, polar wander, Mesozoic convection and the geoid. Nature 297, 391–393.

Anderson, T., 2002. Correction of common lead in U–Pb analyses that do not report ^{204}Pb. Chem. Geol. 192, 59–79.

Andersen, T., Griffin, W.L., Pearson, N.J., 2002. Crustal evolution in the SW part of the Baltic Shield: the Hf isotope evidence. J. Petrol. 43, 1725–1747.

Anhui (Anhui Bureau of Geology and Mineral Resources), 1987. Regional Geology of Anhui Province. Geological Publishing House, Beijing.

Bizimis, M., Sen, G., Salters, V.J.M., 2003. Hf–Nd isotope decoupling in the oceanic lithosphere: constraints from spinel peridotites from Oahu, Hawaii. Earth Planet. Sci. Lett. 217, 43–58.

Blichert-Toft, J., Albarede, F., 1997. The Lu–Hf geochemistry of chondrites and the evolution of the mantle-crust system. Earth Planet. Sci. Lett. 148, 243–258 (Erratum, 154, 349).

Chappell, B.W., White, J.R., 2001. Two contrasting granite types: 25 years later. Aust. J. Earth Sci. 48, 489–499.

Charvet, J., Shu, L.S., Shi, Y.S., Guo, L.Z., Faure, M., 1996. The building of south China: collision of Yangzi and Cathaysia blocks, problems and tentative answers. J. Southeast Asian Earth Sci. 13, 223–235.

Chen, J.F., Foland, K.A., Xing, F.M., Xu, X., Zhou, T.X., 1991. Magmatism along the southeast margin of the Yangtze and Cathaysia block of China. Geology 19, 815–818.

Chen, J.F., Jahn, B.-m., 1998. Crustal evolution of southeastern China: evidence from Sr, Nd and Pb isotope compositions of granitoids and sedimentary rocks. Tectonophysics 284, 101–133.

Cheng, H., 1993. Geochemistry of Proterozoic island-arc volcanic rocks in Northwest Zhejiang. Geochemica (in Chinese with English abstract) 1, 18–27.

Collins, W.J., 2002. Nature of extensional accretionary orogens. Tectonics 21 (4), 1024, doi:10.1029/2000TC001272.

Condie, K.C., 2001. Mantle Plumes and Their Record in Earth History. Cambridge University Press, Cambridge, UK, p. 305.

Corfu, F., Noble, S.R., 1992. Genesis of the southern Abitibi Greenstone belt, Superior Province, Canada: Evidence from zircon Hf isotope analysis using a single filament technique. Geochim. Cosmochim. Acta 56, 2081–2097.

Corfu, F., Hanchar, J.M., Hoskin, P.W.O., Kinny, P., 2003. Atlas of zircon textures. Rev. Miner. Geochem. 53, 468–500.

Cox, K.G., 1988. The Karoo province. In: Macdougall, J.D. (Ed.), Continental Flood Basalts. Kluwer Academic, Dordrecht, pp. 239–271.

Criss, R.E., Gregory, R.T., Taylor Jr., H.P., 1987. Kinetic theory of oxygen isotope exchange between minerals and water. Geochim. Cosmochim. Acta 51, 952–960.

DePaolo, D.J., 1988. Neodymium Isotope Geochemistry: An Introduction. Springer-Verlag, New York, p. 181.

DePaolo, D.J., Linn, A.M., Schubert, G., 1991. The continental crustal age distribution: Method of determing mantle separation ages from Sm–Nd isotopic data and application to the southwerstern United States. J. Geophys. Res. 96, 2071–2088.

Dewey, J.F., 1988. Extensional collapse of orogens. Tectonics 7, 1123–1139.

Dodson, M.H., 1979. Theory of cooling age. Lectures in Isotope Geology. Springer-Verlag, Berlin, pp. 194–202.

Draut, A.E., Clift, P.D., annigan, R.E., Layne, G., Shimizu, N., 2002. A model for continental crust genesis by arc accretion: rare earth element evidence from the Irish Caledonides. Earth Planet. Sci. Lett. 203, 861–877.

Eiler, J.M., Valley, J.W., Baumgartner, L.P., 1993. A new look at stable isotope thermometry. Geochim. Cosmochim. Acta 57, 2571–2583.

Ernst, R.E., Buchan, K.L., 2003. Recognizing mantle plume in the geological record. Ann. Rev. Earth Planet. Sci. 31, 469–523.

Ferreira, V.P., Valley, J.W., Sial, A.N., Spicuzza, M.J., 2003. Oxygen isotope compositions and magmatic epidote from two contrasting metaluminous granitoids, NE Brazil. Contrib. Miner. Petrol. 145, 205–216.

Geisler, T., Ulonska, M., Schleicher, H., Pidgeon, R.T., van Bronswijk, W., 2001. Leaching and differential recrystallisation of metamict zircon under experimental hydrothermal conditions. Contrib. Miner. Petrol. 141, 53–65.

Geisler, T., Pidgeon, R.T., van Bronswijk, W., Kurtz, R., 2002. Transport of uranium, thorium and lead in metamict zircon under low-temperature hydrothermal conditions. Chem. Geol. 191, 141–154.

Gerdes, A., Montero, P., Bea, F., Fershater, G., Borodina, N., Osipova, T., Shardakova, G., 2002. Peraluminous granites frequently with mantle-like isotope compositions: the continental-type Murzinke and Dzhabyk batholiths of the eastern Urals. Intern. J. Earth Sci. 91, 3–19.

Giletti, B.J., 1986. Diffusion effect on oxygen isotope temperatures of slowly cooled igneous and metamorphic rocks. Earth Planet. Sci. Lett. 77, 218–228.

Green, N.L., Usdansky, S.I., 1986. Ternary-feldspar mixing relations and thermobarometry. Am. Miner. 71, 1100–1108.

Gregory, R.T., Criss, R.E., Taylor Jr., H.P., 1988. Oxygen isotope exchange kinetics of mineral pairs in closed and open systems: applications to problems of hydrothermal alteration of igneous rocks and Precambrian iron formation. Chem. Geol. 75, 1–42.

Griffin, W.L., Pearson, N.J., Belousova, E., Jackson, S.E., van Achterbergh, E., O'Reilly, S.Y., Shee, S.R., 2000. The Hf isotope composition of cratonic mantle: LAM-MC-ICPMS analysis of zircon megacrysts in kimberlites. Geochim. Cosmochim. Acta 64, 133–147.

Griffin, W.L., Wang, X., Jackson, S.E., Pearson, N.J., O'Reilly, S.Y., Xu, X., Zhou, X., 2002. Zircon chemistry and magma mixing, SE China: in-situ analysis of Hf isotopes. Tonglu and Pingtan igneous complexes. Lithos 61, 237–269.

Hanchar, J.M., Hoskin, P.W.O., 2003. Zircon. Rev. Miner. Geochem. 16, 1–500.

Harmon, R.S., Hoefs, J., 1995. Oxygen isotope heterogeneity of the mantle deduced from global ^{18}O systematics of basalts from different geotectonic settings. Contrib. Miner. Petrol. 120, 95–114.

Harris, N.B.W., Inger, S., 1992. Trace element modeling of pelite-derived granites. Contrib. Miner. Petrol. 110, 46–56.

Hawkins, J.W., 2003. Geology of supra-subduction zones- Implications for the origin of ophiolites. In: Dilek, Y., Newcomb, S. (Eds.), Ophiolite Concept and the Evolution of Geological Thought: Boulder, Colorado. Geol. Soc. Am. Spec. Paper 373, pp. 227–268.

Hill, R.I., 1991. Starting plumes and continental break-up. Earth Planet. Sci. Lett. 104, 398–416.

Hoefs, J., 2004. Stable Isotope Geochemistry, 5th ed. Springer-Verlag, Berlin, Heidelberg, p. 244.

Holbrook, W.S., Lizarralde, D., McGeary, S., Bangs, N., Diebold, J., 1999. Structure and composition of the Aleutian island arc and implications for continental crust growth. Geology 27, 31–34.

Iizuka, T., Hirata, T., 2005. Improvements of precision and accuracy in in situ Hf isotope microanalysis of zircon using the laser ablation-MC-ICPMS technique. Chem. Geol. 220, 121–137.

Jacobsen, S.B., 1988. Isotopic and chemical constraints on mantle–crust evolution. Geochim. Cosmochim. Acta 52, 1341–1350.

Jahn, B.-m., Condie, K.C., 1995. Evolution of the Kaapvaal Craton as viewed from geochemical and Sm–Nd isotopic analyses of intracratonic pelites. Geochim. Cosmochim. Acta 59, 2239–2258.

Keay, S., Steele, D., Compston, W., 1999. Identifying granite sources by SHRIMP U–Pb zircon geochronology: an application to the Lachlan fold belt. Contrib. Miner. Petrol. 137, 323–341.

Kelemen, P.B., Hanghoj, K., Greene, A.R., 2003. One view of the Geochemistry of subduction-related magmatic arcs, with an emphasis on primitive andesite and lower crust. Treatise Geochem. 3, 593–660.

Kemp, A.I.S., Hawkesworth, C.J., 2003. Granitic perspectives on the generation and secular evolution of the continental crust. Treatise Geochem. 3, 349–410.

Le Pichon, X., Huchon, P., 1984. Geoid, Pangea and convection. Earth Planet. Sci. Lett. 67, 123–135.

Li, X.H., Zhou, G.Q., Zhao, J.X., Fanning, C.M., Compston, W., 1994. SHRIMP ion microprobe zircon U–Pb age and Sm–Nd isotopic charactristics of the NE Jiangxi ophiolite and its tectonic implications. Chin. J. Geochem. 13, 317–325.

Li, Z.X., Zhang, L.H., Powell, C.M., 1995. South China in Rodinia: part of the missing link between Australia-East Antarctica and Laurentia? Geology 23, 407–410.

Li, X.H., Zhao, J.X., McCulloch, M.T., Zhou, G.Q., Xing, F.M., 1997. Geochemical and Sm–Nd isotopic of Neoproterozoic ophiolites from southeastern China: petrogenesis and tectonic implications. Precambr. Res. 81, 129–144.

Li, X.H., 1999. U–Pb zircon ages of granites from the southern margin of the Yangtze Block: timing of Neoproterozoic Jinning orogeny in SE China and implications for Rodinia Assembly. Precambr. Res. 97, 43–57.

Li, Z.X., Li, X.H., Kinny, P.D., Wang, J., 1999. The breakup of Rodinia: did it start with a mantle plume beneath South China? Earth Planet Sci. Lett. 173, 171–181.

Li, Z.-X., Li, X.H., Zhou, H., Kinny, P.D., 2002a. Grenville-aged continental collision in South China: new SHRIMP U–Pb zircon results and implications for Rodinia configuration. Geology 30, 163–166.

Li, X.H., Liu, Y., Tu, X.L., Hu, G.Q., Zeng, W., 2002b. Precise determination of chemical compositions in rock samples using ICP-AES and ICP-MS: a comparative study of sample digestion techniques of alkali fusion and acid dissolution. Geochimica (in Chinese with English abstract) 31, 289–294.

Li, W.X., Li, X.H., 2003. Adakitic granites within the NE Jiangxi ophiolites, South China: geochemical and Nd isotopic evidence. Precambr. Res. 122, 29–44.

Li, X.H., Li, Z.X., Ge, W.C., Li, W.X., Liu, Y., Wingate, M.T.D., 2003a. Neoproterozoic granitoids in South China: crustal melting above a mantle plume at ca. 825 Ma? Precambr. Res. 122, 45–83.

Li, Z.X., Li, X.H., Kinny, P.D., Wang, J., Zhang, S., Zhou, H., 2003b. Geochronology of Neoproterozoic syn-rift magmatism in the Yangtze Craton, South China and correlations with other continents: evidence for a mantle superplume that broke up Rodinia. Precambr. Res. 122, 85–109.

Li, W.X., Li, X.-H., Li, Z.-X., 2005. Neoproterozoic bimodal magmatism in the Cathaysia Block of South China and its tectonic significance. Precambr. Res. 136, 51–66.

Ludwig, K.R., 1998. On the treatment of concordant uranium-lead ages. Geochim. Cosmochim. Acta 62, 665–676.

Ludwig, K.R., 2001. Users Manual for Isoplot/Ex (rev. 2.49): A Geochronological Toolkit for Microsoft Excel. Berkeley Geochronology Center, Special Publication, No. 1a, p. 55.

McCulloch, M.T., Chappell, B.W., 1982. Nd isotope characteristics of S- and I-type granites. Earth Planet. Sci. Lett. 58, 51–64.

McDonough, W.F., Sun, S.S., 1995. The composition of the earth. Chem. Geol. 120, 223–253.

Middlemost, E.A.K., 1994. Naming materials in the magma/igneous rock system. Earth Sci. Rev. 37, 215–224.

Miller, C.F., McDowell, S.M., Mapes, R.W., 2003. Hot and cold granite? Implications of zircon saturation temperatures and preservation of inheritance. Geology 31, 529–532.

Morgan, W.J., 1981. Hotspot tracks and the opening of the Atlantic and Indian Oceans. In: Emiliani, C. (Ed.), The Sea. Wiley, New York, pp. 443–487.

Nowell, G.M., Kempton, P.D., Noble, S.R., Fitton, J.G., Saunders, A.D., Mahoney, J.J., Taylor, R.N., 1998. High precision Hf isotope measurements of MORB and OIB by thermal ionisation mass spectrometry: insights into the depleted mantle. Chem. Geol. 149, 211–233.

O'Neil, J.R., Chappell, B.W., 1977. Oxygen and hydrogen isotope relations in the Berridale batholith. J. Geol. Soc. London 133, 559–571.

Patino Douce, A.E., McCarthy, T.C., 1998. Melting of crustal rocks during continental collision and subduction. In: Hacker, B.R., Liou, J.G. (Eds.), When Continents Collide: Geodynamics and Geochemistry. Kluwer Academic Publishers, Dordrecht, pp. 27–55.

Piotrowski, A.M., Lee, D.-C., Christensen, J.N., Burton, K.W., Halliday, A.N., Hein, J.R., Guenther, D., 2000. Changes in erosion and ocean circulation recorded in the Hf isotopic compositions of North Atlantic and Indian Ocean ferromanganese crusts. Earth Planet. Sci. Lett. 181, 315–325.

Richards, M.A., Duncan, A.R., Courtillot, V.E., 1989. Flood basalts and hot-spot tracks plume heads and tails. Science 246, 103–107.

Rudnick, R.L., 1995. Making continental crust. Nature 378, 571–578.

Samson, S.D., D'Lemos, R.S., Blichert-Toft, J., Vervoort, J., 2003. U–Pb geochronology and Hf–Nd isotope compositions of the oldest Neoproterozoic crust within the Cadomian orogen: new evidence for a unique juvenile terrane. Earth Planet. Sci. Lett. 208, 165–180.

Scherer, E., Munker, C., Mezger, K., 2001. Calibration of the lutetium-hafnium clock. Science 293, 683–687.

Shen, W.Z., Ling, H.F., Li, W.X., Huang, X.L., Wang, D.Z., 1999. Study on the Nd–Sr isotopic compositions of granitoids in SE China. Geol. J. China Univ. (in Chinese with English abstract) 5 (1), 22–32.

Storey, B.C., Alabaster, T., Hole, M.J., Pankhurst, R.J., Wever, H.E., 1992. Role of subduction-plate boundary forces during the initial stages of Gondwana break-up: evidence from the proto-Pacific margin of Antarctica. In: Storey, B.C., Alabaster, T., Pankhurst, R.J. (Eds.), Magmatism and the Causes of Continental Break-up. Spec. Pub. Geol. Soc. Lond. 68, pp. 149–164.

Storey, B.C., Kyle, P.R., 1997. An active mantle mechanism for Gondwana breakup. South Africa J. Geol. 100, 283–290.

Sun, S.S., McDonough, W.F., 1989. Chemical and isotopic systematics of oceanic basalt: implications for mantle composition and processes. In: Saunders, A.D., Norry, M.J. (Eds.), Magmatism in the Ocean Basins. Geol. Soc. Spec. Publ. 42, pp. 528–548.

Sylvester, P.J., 1998. Post-collisional strongly peraluminous granites. Lithos 45, 29–44.

Thompson, A.B., Connolly, J.A.D., 1995. Melting of the continental crust: some thermal and petrologic constraints on anatexis in continental collision zones and other tectonic settings. J. Geophys. Res. 100, 15565–15579.

Tommasi, A., Vauchez, A., 2001. Continental rifting parallel to ancient collisional belts: an effect of the mechanical anisotropy of the lithospheric mantle. Earth Planet. Sci. Lett. 185, 199–210.

Valley, J.W., Kitchen, N., Kohn, M.J., Niendorf, C.R., Spicuzza, M.J., 1995. UWG-2, a garnet standard for oxygen isotope ratio: strategies for high precision and accuracy with laser heating. Geochim. Cosmochim. Acta 59, 5223–5231.

Valley, J.W., Kinny, P.D., Schulze, D.J., Spicuzza, M.J., 1998. Zircon metacryst from kimberlite: oxygen isotope variability among mantle melts. Contrib. Miner. Petrol. 133, 1–11.

Valley, J.W., 2003. Oxygen isotopes in zircon. Rev. Miner. Geochem. 53, 343–385.

van de Flierdt, T., Frank, M., Lee, D.C., Halliday, A.N., 2002. Glacial weathering and the hafnium composition of seawater. Earth Planet. Sci. Lett. 198, 167–175.

Vauchez, A., Barruol, G., Tommasi, A., 1997. Why do continents break-up parallel to ancient orogenic belts? Terra Nova 9, 62–66.

Vervoort, J.D., Blichert-Toft, J., 1999. Evolution of the depleted mantle: Hf isotope evidence from juvenile rocks through time. Geochim. Cosmochim. Acta 63, 533–556.

Vervoort, J.D., Patchett, P.J., Blichert-Toft, J., Albarede, F., 1999. Relationship between Lu–Hf and Sm–Nd isotopic systems in the global sedimentary system. Earth Planet. Sci. Lett. 168, 79–99.

Vervoort, J.D., Patchett, J.P., Albarede, F., Blichert-Toft, J., Rudnick, R., Downes, H., 2000. Hf–Nd isotopic evolution of the lower crust. Earth Planet. Sci. Lett. 181, 115–119.

Wang, J., Li, Z.X., 2003. History of Neoproterozoic rift basins in South China: implications for Rodinia break-up. Precambr. Res. 122, 141–158.

Wang, J., Li, X.H., Duan, T.Z., Liu, D.Y., Song, B., Li, Z.X., Gao, Y.H., 2003a. Zircon SHRIMP U–Pb dating for the Cangshuipu volcanic rocks and its implications for the lower boundary age of the Nanhua strata in South China. Chin. Sci. Bull. 48, 1663–1669.

Wang, J., Li, Z.X., Duan, T.Z., Zhang, S.H., Bao, C.M., Li, Z.X., Gao, Y.H., Mou, C.L., 2003b. Stratigraphic and sedimentological records of the Neoproterozoic rift basins in southern China. In: Li, Z.X., Wang, J., Li, X.H. (Eds.), From Sibao Orogenesis to Nanhua Rifting: Late Precambrian Tectonic History of Eastern South China—An Overview and Field Guide. Geological Pubishing House, Beijing, pp. 26–39.

Wang X.L., Zhou J.C., Qiu H.S., Gao H.F., 2004a. Comment on Neoproterozoic granitoids in South China: crustal melting above a mantle plume at ca. 825 Ma? by X.-H. Li et al. Precambr. Res. 132, 401–403.

Wang, X.L., Zhou, J.C., Qiu, J.S., Gao, J.F., 2004b. Geochemistry of the Meso- to Neoproterozoic basic-acid rocks from Hunan Province, South China: implications for the evolution of the western Jiangnan orogen. Precambr. Res. 135, 79–103.

Watson, E.B., Harrison, T.M., 1983. Zircon saturation revisited: temperature and composition effects in a variety of crustal magma types. Earth Planet. Sci. Lett. 64, 295–304.

Watson, E.B., Cherniak, D.J., 1997. Oxygen diffusion in Zircon. Earth Planet. Sci. Lett. 148, 527–544.

White, R.S., 1997. Mantle plume origin for the Karoo and Ventersdorp flood basalts, South Africa. South Africa. J. Geol. 100, 271–282.

Wiedenbeck, M., Alle, P., Corfu, F., Griffin, W.L., Meier, M., Oberli, F., von Quadt, A., Roddick, J.C., Spiegel, W., 1995. Three natural zircon standards for U–Th–Pb, Lu–Hf, trace element and REE analyses. Geostand. Newslett. 19, 1–23.

Woodhead, J., Hergt, J., Shelley, M., Eggins, S., Kemp, R., 2004. Zircon Hf-isotope analysis with an excimer laser, depth profiling, ablation of complex geometries, and concomitant age estimation. Chem. Geol. 209, 121–135.

Xie, G.G., Li, J.H., Li, W.X., Tang, H.F., Li, H.M., Zhou, X.M., 1997. U–Pb zircon dating of presinian rocks at Lushan Mt. and its geological implication. Sci. Geol. Sin. (in Chinese with English abstract) 32 (1), 110–115.

Xing, F.M., Xu, X., Ren, S.M., Li, Y.Y., 1988. Petrochemistry, formation age and conditions of the Shexian intrusion in southern Anhui Province. Geol. Rev. (in Chinese with English abstract) 34 (4), 400–413.

Xu, P., Wu, F.-y., Xie, L.-w., Yang, Y.-h., 2004. Hf isotopic compositions of the standard zircons for U–Pb dating. Chin. Sci. Bull. 49, 1642–1648.

Yuan, H.-L., Gao, S., Liu, X.-M., Li, H.-M., Gunther, D., Wu, F.-Y., 2004. Accurate U–Pb age and trace element determinations of zircon by laser ablation-inductively coupled plasma mass spectrometry. Geostand. Newsl. 28, 353–370.

Zhao, G.-C., Cawood, P.A., 1999. Tectonothermal evolution of the Mayuan assemblage in the Cathaysia Block: implications for Neoproterozoic collision-related assembly of the South China craton. Am. J. Sci. 299, 309–339.

Zhao, Z.-F., Zheng, Y.-F., 2003. Calculation of oxygen isotope fractionation in magmatic rocks. Chem. Geol. 193, 59–80.

Zhao, Z.-F., Zheng, Y.-F., Wei, C.-S., Gong, B., 2004. Temporal relationship between granite cooling and hydrothermal uranium mineralization at Dalongshan in China: a combined radiometric and oxygen isotopic study. Ore Geol. Rev. 25, 221–236.

Zheng, Y.-F., 1989. Influence of the nature of the initial Rb–Sr system on isochron validity. Chem. Geol. 80, 1–16.

Zheng, Y.-F., 1990. A further three-dimensional U–Pb method for solving the two-stage episodic model. Geochem. J. 24, 29–37.

Zheng, Y.-F., 1991. Calculation of oxygen isotope fractionation in metal oxides. Geochim. Cosmochim. Acta 55, 2299–2307.

Zheng, Y.-F., 1992. The three-dimensional U–Pb method: Generalized models and implications for U–Pb two-stage systematics. Chem. Geol. 100, 3–18.

Zheng, Y.-F., 1993a. Calculation of oxygen isotope fractionation in anhydrous silicate minerals. Geochim. Cosmochim. Acta 57, 1079–1091.

Zheng, Y.-F., 1993b. Calculation of oxygen isotope fractionation in hydroxyl-bearing silicates. Earth Planet. Sci. Lett. 120, 247–263.

Zheng, Y.-F., Fu, B., 1998. Estimation of oxygen diffusivity from anion porosity in minerals. Geochem. J. 32, 71–89.

Zheng, Y.-F., 1999. On calculation of oxygen isotope fractionation in minerals. Episodes 22, 99–106.

Zheng, Y.-F., Wang, Z.R., Li, S.G., Zhao, Z.F., 2002. Oxygen isotope equilibrium between eclogite minerals and its constraints on mineral Sm–Nd chronometer. Geochim. Cosmochim. Acta 66, 625–634.

Zheng, Y.-F., Fu, B., Gong, B., Li, L., 2003a. Stable isotope geochemistry of ultrahigh Pressure metamorphic rocks from the Dabie-Sulu orogen in China: Implications for geodynamics and fluid regime. Earth Sci. Rev. 62, 105–161.

Zheng, Y.-F., Zhao, Z.F., Li, S.G., Gong, B., 2003b. Oxygen isotope equilibrium ultrahigh-pressure metamorphic minerals and its constraints on Sm–Nd and Rb–Sr chronometers. In: Vance, D., Muller, W., Villa, I. (Eds.), Geochronology: Linking the Isotope Record with Petrology and Textures. Geological Society Special Publications, 220, pp. 93–117.

Zheng, Y.-F., Wu, Y.B., Chen, F.K., Gong, B., Li, L., Zhao, Z.F., 2004. Zircon U–Pb and oxygen isotope evidence for a large-scale ^{18}O depletion event in igneous rocks during the Neoproterozoic. Geochim. Cosmochim. Acta 68, 4145–4165.

Zheng, Y.-F., Wu, Y.-B., Zhao, Z.-F., Zhang, S.-B., Xu, P., Wu, F.-Y., 2005. Metamorphic effect on zircon Lu–Hf and U–Pb isotope systems in ultrahigh-pressure eclogite-facies metagranite and metabasite. Earth Planet. Sci. Lett. 240, 378–400.

Zheng, Y.-F., Zhao, Z.-F., Wu, Y.-B., Zhang, S.-B., Liu, X.M., Wu, F.-Y., 2006. Zircon U–Pb age, Hf and O isotope constraints on protolith origin of ultrahigh-pressure eclogite and gneiss in the Dabie orogen. Chem. Geol., doi:10.1016/j.chemgeo.2006.01.005.

Zhou, X.M., Wang, D.Z., 1988. The peraluminous granodiorites with low initial $^{87}Sr/^{86}Sr$ ratio and their genesis in southern Anhui province, eastern China. Acta Petrol. Sin. (in Chinese with English abstract) 4 (3), 37–45.

Zhou, X.M., Zou, H.B., Yang, J.D., Wang, Y.X., 1989. Sm–Nd isochron age of the Fuchuan Ophiolite Suite in Shexian, Anhui Province and its geological significance. Chin. Sci. Bull. (in Chinese) 16, 1243–1245.

Zhou, M.F., Yan, D.-P., Kennedy, A.K., Li, Y.-Q., Ding, J., 2002a. SHRIMP U–Pb zircon geochronological and geochemical evidence for Neoproterozoic arc-magmatism along the western margin of the Yangtze Block, South China. Earth Planet. Sci. Lett. 196, 51–67.

Zhou, M.F., Kennedy, A.K., Sun, M., Malpas, J., Lesher, C.M., 2002b. Neoproterozoic arc-related mafic intrusions along the northern margin of South China: implications for the accretion of Rodinia. J. Geol. 110, 611–618.

Zhou, J.C., Wang, X.L., Qiu, J.S., Gao, J.F., 2004. Geochemistry of Meso- and Neoproterozoic mafic-ultramafic rocks from northern Guangxi, China: Arc or plume magmatism? Geochem. J. 38, 139–152.